# EXPERIMENTAL INVESTIGATION OF DROPLET IMPACT ON MOVING SURFACES

A Thesis

by

Gökhan Kayansalçik

Submitted to the
Graduate School of Sciences and Engineering
In Partial Fulfillment of the Requirements for
the Degree of

Master of Science

in the
Department of Mechanical Engineering

Özyeğin University
January 2018

**EXPERIMENTAL INVESTIGATION OF DROPLET IMPACT ON MOVING SURFACES**

Approved by:


Asst. Prof. Dr.-Ing Özgür Ertunç, Advisor
Department of Mechanical Engineering
*Özyeğin University*

Prof. Dr. Metin Muradoğlu
Department of Mechanical Engineering
*Koç University*

Asst. Prof. Altuğ Başol
Department of Mechanical Engineering
*Özyeğin University*



Date Approved: 25 January 2018

*To My Family*

# ABSTRACT

Droplet impact on moving surfaces has been studied experimentally by using high-speed photography technique. Fluid properties (droplet diameter and velocity), surface properties (wettability and roughness) and surface velocity have been altered. Distilled water was used as working fluid. Hydrophilic, hydrophobic and superhydrophobic surfaces which have different roughness levels have been used in the experiments to understand the effect of wettability and roughness on droplet behavior. In addition to droplet behavior, effect of $We_n$, $We_t$ and contact angle on droplet spreading in radial and tangential directions have been studied on hydrophilic and hydrophobic surfaces. Dynamic and static contact angle have been measured. Dynamic contact angle which consists of advancing and receding contact angle have been measured using tilting plate technique and static contact angle has been measured by using sessile drop method. Moreover, roughness of the surfaces have been measured by using white light interferometry and topology plots have been created. As a result, various types of rebound, deposition and splitting mechanisms have been investigated depending on the $We_n$, $We_t$ and surface properties. Regime maps have been created for each wettability and roughness as a function of $We_n$ and $We_t$. Furthermore, radial, tangential and area spread factor figures have been presented as a function of nondimensional time for each contact angle at different $We_n$ and $We_t$.

# ÖZETÇE

Hareketli yüzeyler üzerindeki damlacık davranışı , yüksek hızlı fotoğraf tekniği kullanılarak deneysel olarak incelenmiştir. Sıvı özellikleri (damla çapı ve hızı), yüzey özellikleri (ıslanabilirlik ve pürüzlülük) ve yüzey hızı değiştirilmiştir. Çalışma sıvısı olarak saf su kullanılmıştır. Deneylerde su seven, sevmeyen, super sevmeyen ve farklı pürüzlülüklerdeki yüzeyler kullanılmış olup bu özelliklerin damla davranışları üzerindeki etkisi gözlemlenmiştir. Damla davranışına ek olarak, kontak açısı, normal ve teğetsel Weber numarasnn radyal ve teğetsel yöndeki damla yayılmasına olan etkisi su seven ve sevmeyen yüzeylerde incelenmiştir. Yüzeylerin dinamik ve statik temas açısı ölçülmüştür. Yayılma ve toplanmadan oluşan dinamik kontak açısı "tilting plate" tekniği, statik temas açısı ise "sessile drop" yöntemi kullanılarak ölçülmüştür. Buna ek olarak, yüzey pürüzlülük ölçümleri "white light interferometry" kullanılarak yapılmış olup yüzey topoloji çizimleri yapılmıştr. Normal, teğetsel Weber numaraları ve yüzey özelliklerine bağlı olarak geri zıplama, yayılma ve parça kopması mekanizmaları araştırılmıştır. Bu araştrmalar sonucunda her ıslanabilirlik ve pürüzlülük için normal ve teğetsel Weber numarasına bağlı olarak rejim haritaları oluşturulmuştur. Ayrıca, her kontak açısı için radyal, teğetsel ve alan dağılım faktörü, farklı normal ve teğetsel Weber sayısında boyutsuz zamanın bir fonksiyonu olarak sunulmuştur

# ACKNOWLEDGEMENTS

I appreciate my supervisor, Dr. Ing. Özgür Ertunç on behalf of his generous supports since this work would be impossible without the help of him. Additionally, I am so thankful of my family because of their supports and encouragements, which were a thrust for me during this period. Finally, I thank all whom helped me during this period. I hope this friendship will last forever.

The study was supported by the Scientific and Technological Research Council of Turkey (TÜBİTAK), Project No:114M423. Prof. Dr. Mehmet Arık for lending the high speed camera to us for visualization. Assoc. Prof. Dr. Bahar Başım for valuable comments on the surface preparation. KUYTAM for providing surface roughness measurement service.

# TABLE OF CONTENTS

# LIST OF TABLES

# LIST OF FIGURES

# CHAPTER I

# INTRODUCTION

Droplet impingement phenomenon has many technical applications such as surface coating, ink-jet printing, rapid spray cooling of hot surfaces, internal combustion engines and so on and so forth. Since this has been used in many applications, many people who are physicist, engineer or mathematician have been working on this subject. Most of the studies about the subject have been published on the dry stationary surface case. However, there is not much study on the droplet interaction with moving surfaces. Therefore, literature survey of the topic will be examined in two sections as stationary and moving surfaces.

## *1.1 Droplet Behavior on Stationary Surfaces*

A droplet can behave six different types when it hits to the solid dry surface[1]. These behaviors are deposition, prompt splash, corona splash, receding breakup, partial rebound and rebound. In the deposition, droplet hits and spreads onto the surface. The next behavior is prompt splash, when the droplet hits the surface, it may create splashes around droplet asymmetrically and this behavior called as prompt splash. However in corona splash, it hits to surface and creates rim then it creates splashes but it is formed as corona shape and because of this it is called corona splash. In receding break-up, the droplet hits to surface and fingering formation is seen around the lamella. Then splitting is observed, while lamella is receding, no splashing occurs. Furthermore, partial rebound occurs when the droplet hits the surface, it creates lamella and starts to elongate to the upward (jet creation) and then some part of the droplet leaves from the rest. The last type is the complete rebound, in this type it hits and spreads on the surface then it rebounds completely by losing its initial formation.

Moreover, development of the droplet when it hits to surface has been investigated and the time evolution of the spread factor consists of four stages. These are kinematic phase, the spreading phase, a relaxation phase and a wetting/ equilibrium phase[2].

Kinematic phase is the early stage of impact, the shape of drop resembles a truncated sphere and no spreading lamella is yet visible[2]. Inertia and surface reaction forces are dominant when droplet just hits to the surface. In the spreading phase, lamella is ejected from the base of the drop and forms a thin film bounded by a rim. In addition to inertia and reaction of the surface, viscous forces, surface tension forces and intermolecular forces at the interface affect droplet in the spreading phase. After spreading phase, relaxation phase starts and the drop may begin to recede depending on the dynamic contact angle of the surface. Inertial force eliminated and the other forces still affects the droplet in relaxation phase. The last phase is the wetting/equilibrium phase where droplet consumes all its energy and reaches to the equilibrium. Inertial, viscous and surface reaction forces are eliminated and gravitational force starts to influence on droplet in addition to the other forces.

After the kinetic energy of the drop impact has been partly dissipated by the viscous forces and spread on the surface, behavior of the lamella determined by the surface wettability[3]. It describes the ability of a liquid to spread on a solid in a surrounding gas phase and is evaluated by the static contact angle. If $\theta$ is lower than 90° , it shows the partial wettability. If $\theta$ is larger than 90° , it shows no partial wettability. If $\theta$= 0° , wetting and if $\theta$=180° , it demonstrates non-wetting. Likewise, dynamic contact angles which are advancing and receding contact angles influence the behavior of droplet and they are used to calculate the contact angle hysteresis ($\theta_{adv}$- $\theta_{adv}$). In addition to these parameters, surface roughness also affects the behavior of droplet. There are two parameters for the roughness; the first one is the roughness wavelength $R_w$ and shorter wavelength causes prompt splash at high impact velocities. The second one is roughness amplitude $R_a$ and higher the roughness amplitude, causes the prompt splash[1].

Furthermore, droplet behavior can be determined by using dimensionless numbers which are Reynolds number, Weber number, Capillary number, Ohnesorge number and Bond number. These can be calculated by using inertial, viscous, surface tension and gravitational forces.

## 1.2 Droplet Behavior on Moving Surfaces

Droplet spreading, splashing and behavior on moving surfaces have been investigated by the limited number of studies when it is compared with the stationary surface case[4,5].

Deformation and splashing of the droplet onto moving smooth and rough surface has been visualized and explained[4]. Empirical model has been formulated to predict whether the impacted monodisperse droplets will splash or deposit when they hit to the rotating disk by using a correlation constant K which can be found by using Re and Oh numbers. Also, by using phase Doppler anemometer, diameter and velocity distributions of splashing phenomena was examined. Fluid properties (viscosity and surface tension) and kinematic parameters (velocity and size of primary droplet) effects the diameter of secondary droplets for impingement on smooth surface case. On the other hand, in case of an impingement on rough surface, non-dimensional surface roughness number (St) determines the distributions. Moreover, impingement kinematics has a significant effect on the velocity distribution of droplets and it is supplied by the tangential impact velocity for the smooth and rough surface. Since the corona formation causes energy dissipation, normal momentum is partially conserved. Splashing occurs under the influence of local surface angle, leading to a transfer of tangential momentum into normal momentum. Because of this, the mean reflection angle to the normal of the secondary droplets decreases on the rough surface.

Moreover, behavior of droplet has been studied on Teflon surface by looking Weber number[6]. A train of water droplets have been impacted to the rotating cylindrical Teflon surface. The impact resulted in partial rebound, deposition and split deposition. Regime map was created as a function of normal and tangential Weber number. So, by looking Weber numbers which composed of normal and tangential velocities, the behavior of the droplet can be predicted.

$$We_n = \frac{\rho V_{droplet}^2 D_{droplet}}{\sigma} \tag{1}$$

$$We_t = \frac{\rho V_{surface}^2 D_{droplet}}{\sigma} \tag{2}$$

In partial rebound, it is creates lamella and start to elongate to upward (jet creation) and then some of the droplet leaves from the rest. For the second case which is deposition, droplet hits to the surface at the low energy and spreads on the surface. Similarly, same phenomena can be seen at the medium tangential Weber numbers. Lastly, if tangential Weber number of the surface is high, it divides droplet into two pieces. Also, the shape of the impacted droplet at the maximal spread determines the impact regime boundaries. If the long axis 1.1 times the short axis, partial rebound turns into deposition. In the other case, when long axis 1.46 times the short axis, partial rebound changes to the split deposition[6]. In the study, not only droplet behavior has been studied but also spread area of the impacted droplet has been investigated and found out that when the tangential Weber number increased, spread area of the droplet increases.

Splashing phenomena on the moving surface has been studied[7]. In the study, whether tangential velocity will prevent or cause splashing has been studied and a model has been developed to find out the splashing threshold. Ethanol droplets were collided to moving surfaces which moves different speed and direction. Depending on the magnitude of tangential velocity, droplet can behave three different ways; the lamella may spread in all directions, splash in all direction and asymmetrically splashing. If there is no tangential velocity there will be spread or splash in all directions, there will not be observed asymmetric splashing.

In addition, drop spreading, splashing and behavior onto moving smooth hydrophilic and hydrophobic surface have been studied[5]. Drops have been generated using liquids which have different viscosities. Drop impact phenomena was examined in two stages that are lamella extension and lamella retraction. At the first stage, it was observed that lamella spreads over the moving surface asymmetrically and at the early stages of the impact, drop solely moves in vertical direction. So, center of drop stays at the same position while lamella spreads asymmetrically. Also, importance of the contact angle hysteresis and receding contact angle of the surface have been notified in the lamella retraction stage. If the contact angle hysteresis high, $\Delta t$ which is pinning time increases and pinning time is the time for the change in contact angle from advancing to receding. Similarly, receding contact angle is crucial because it influences the velocity of contact line while receding. So, hysteresis and receding contact angle determines the when and how recoils lamella. Additionally, it was found that splashing in the moving surface case is not a 1D phenomenon, it should have been in 2D and a model developed for azimuthally asymmetric splashing as a function of $Ca_n$, $We_n$, drop velocity, surface velocity and contact angle. Lastly, regime maps have been created for behavior of drops onto the moving hydrophobic and hydrophilic surfaces for both stages of impact.

## *1.3 Open Questions in the Literature*

In the literature, splashing on moving surface has been studied by Mundo et.al[4] and Bird et.al[7]. However, they did not study effect of the wettability on splashing. There are some studies about the influence of $We_n$ and $We_t$ on droplet impact outcome onto moving surface. Chen and Wang studied on hydrophobic smooth surface[6] and Almohammadi and Amirfazli worked on hydrophobic and hydrophilic smooth surfaces[5].

However, both studies did not find out the effect of roughness to droplet behavior. Range and resolution of the regime maps differs from each other. Chen and Wang have done experiments in smaller range but more data has been collected whereas Almohammadi and Amirfazli have done less experiments but in the higher range of $We_n$ and $We_t$. In addition to these, droplet behavior on moving superhydrophobic surfaces which have different roughness levels has not been examined in the literature.

## *1.4 Objectives of the Present Investigations*

The present study answers questions about the droplet behavior and spreading onto moving surfaces. The effects of $We_n$ and $We_t$, surface wettability and roughness on the behavior of droplets have been sought.

The following outcomes are expected on moving surfaces. Impacted droplet onto the moving surface cannot be affected too much by the movement at the low surface velocities and it will behave similar to the stationary surfaces. On the other hand, when the velocity of the surface increased, the droplet will elongate because of the motion. If the elongation of the impacted droplet is sufficient enough, droplet can split depending on the tangential Weber number and properties of the surface. Also, wettability of the surface will influence the behavior of droplet. On hydrophilic surface, droplet hits to the surface and spreads, so the behavior is supposed to be types of deposition[5]. For the hydrophobic surface, it is supposed to deposit, partially rebound and deposit while splitting depending on the fluid properties and surface velocity[5,6]. Lastly, when droplet hits to the superhydrophobic surface, it cannot stick to surface so it is supposed to rebound and types of rebound can be seen as behavior. Furthermore, surface roughness and direction of the surface motion will affect the generation of secondary droplets. If the surface is rough, splashing may occur depending on the local surface angle[4]. Splashing direction depends on velocity and direction of the surface. It is tend to move the opposite direction of the surface movement as the tangential velocity increased[7].

When spreading is considered, it is expected that spreading in radial direction increases with $We_n$ and maximum spreading occurs at highest $We_n$ and lowest $We_t$. Tangential spreading rises with $We_t$ and maximum tangential spreading occurs for highest $We_t$ and lowest $We_n$. Contact angle is also a key parameter in droplet impact dynamics. Maximum spread area and elapsed time to reach maximum spreading are dependent on contact angle.

In the present investigations, the effects of moving surfaces with various properties (roughness and contact angle) have been studied on droplet impact outcome and spreading by changing $We_n$ and $We_t$. For this purpose an experimental test rig was built, surfaces were prepared and characterized. Investigations were conducted with the help of high-speed imaging. Range of the present study has larger range than Chen and Wang and smaller range than Almohhamadi and Amirfazli (Figure 1) but more data has been collected than both of the studies to demonstrate the richness of phenomena.

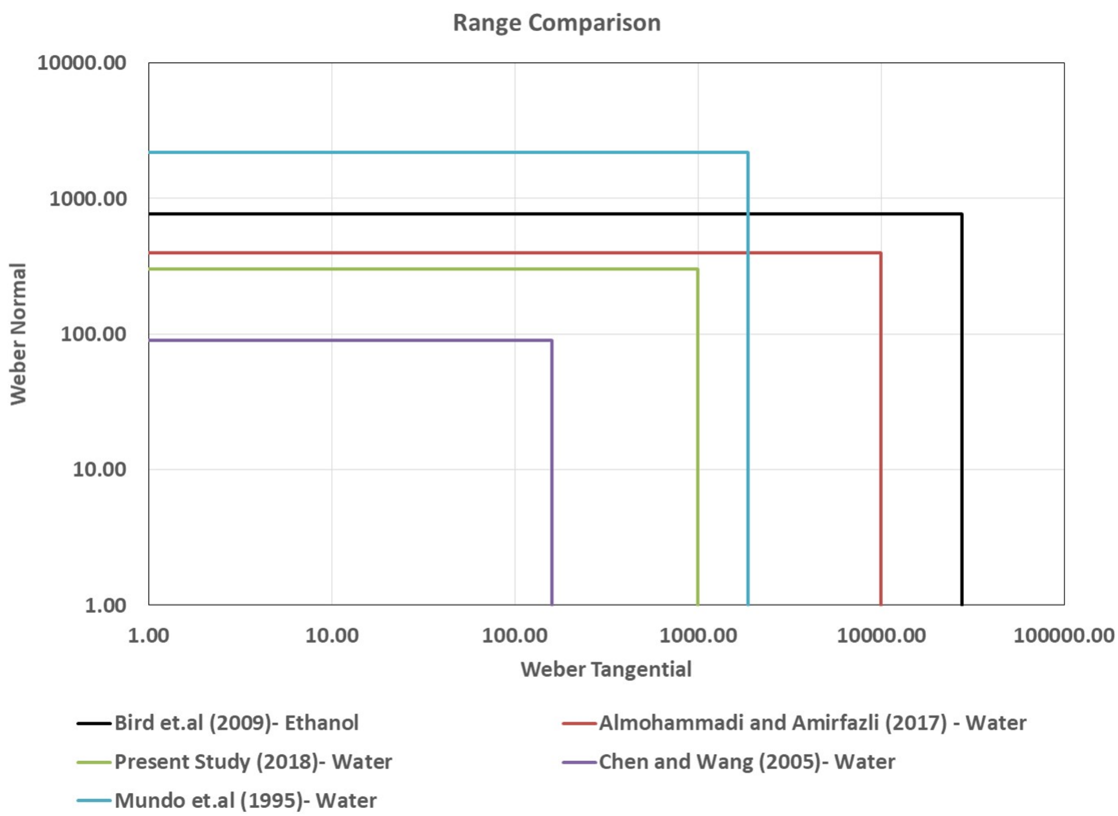


**Figure 1:** Range comparison of the studies with reported contact angles- Mundo et.al.(1995) $\theta_{static}$=75°; Bird et.al.(2005), contact angle was not reported; Chen and Wang (2005) $\theta_{static}$= 103°; Almohammadi and Amirfazli (2017) $\theta_{adv}$=89° $\theta_{rec}$=34°, $\theta_{adv}$=123° $\theta_{rec}$=109°; The present study (2018), contact angles can be seen in table 2.

# CHAPTER II

# EXPERIMENTAL FACILITIES AND OVERVIEW OF EXPERIMENTAL TECHNIQUES

## *2.1 Dynamic Contact Angle Measurement Setup*

Contact angle of the surface is one of the key parameters which affects the droplet behavior. It is the angle formed by the intersection of liquid-solid interface and liquid-vapor interface[8]. In the literature it is reported as static and dynamic contact angle. In the static contact angle, droplet is placed on the surface then angle is measured. The angle gives idea about wettability of the surface. Dynamic contact angle is reported as advancing contact angle which is the angle measured while droplet spreading on the surface and receding contact angle which can be measured while droplet recoiling on the surface. The difference between advancing and receding contact angle gives the hysteresis which affects the pinning time. It is the required time to advancing contact angle turn into receding contact angle. Sessile drop and tilting plate method have been commmonly used to measure dynamic contact angle. Drop deposited on the surface and syringe needle inserted into droplet in the sessile drop method. Then volume addition has been done at very low flow rate until the contact line of the droplet expands and the angle which is just before the contact line expansion recorded as advnacing contact angle. Then, volume extraction begins and volume is extracted at very low flow rate until contact line recedes and the angle just before the contact line movement is recorded as receding contact. In the tilting plate method, drop depositted on the surface and it is tilted slowly, then the frame which is just before the drop slip on the surface taken to measure the advancing and receding contact angle (Figure 2b). Advancing contact angle is measured from leading edge of the droplet whereas receding contact angle is measured from the trailing edge. In our study, static and dynamic contact angle measurements have been done. Static contact angle has been measured by using the method mentioned above and dynamic contact angle has been measured by using tilting plate method. A setup which consists of a servo, syringe with needle, syringe pump and camera has been established to measure the contact angles (Figure 2a).

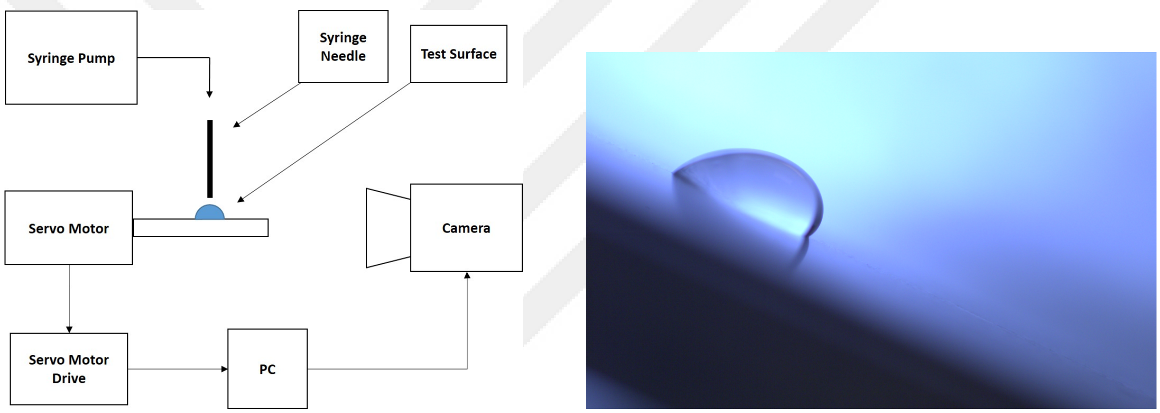


(a) (b)

**Figure 2:** (a) Schema of contact angle measurement setup (b) Example measurement on hydrophobic smooth surface

## *2.2 White Light Interferometry for Surface Roughness*

Roughness of the surfaces have been measured using white light interferometry technique by KUYTAM. White light interferometry is a non-contact optical method to measure height of the structures. $R_a$, $R_z$, $R_t$ and $R_q$ used to quantify the surface roughness. $R_a$ is the average roughness over the entire measured array. $R_z$ is the average of the ten greatest peak to valley separations over the sample. $R_t$ is the peak to valley difference over the entire measured array. $R_q$ is the root mean squared roughness calculated over the entire measured array. In addition to conventional roughness parameters, a nondimensional number $S_t$ has been used to quantify the roughness by

Mundo et.al.[4]. It is the ratio of peak to valley difference over the entire measured array and average initial droplet diameter.

$$R_a = \frac{1}{n}\sum_{i=1}^{n}|Z_i - \bar{Z}| \tag{3}$$

$$R_z = \frac{1}{n}[(H_1 + H_2 + ... + H_n)] - [(L_1 + L_2 + ... + L_n)] \tag{4}$$

$$R_t = R_p - R_v \tag{5}$$

$$R_q = \sqrt{\frac{1}{n}\sum_{i=1}^{n}(Z_i - \bar{Z})^2} \tag{6}$$

$$S_t = \frac{R_t}{D_0} \tag{7}$$

## *2.3 Drop Impact Measurements Setup*

In the experiments, water droplets which have different diameters and velocities have been impacted to a rotating disk to examine the behavior of droplets onto the different surfaces. The experimental setup shown schematically in figure 3 consists of a signal generator, DAQ system, syringe pump, solenoid, high speed cameras, high lumen light, servo motor and a syringe needle. Droplets have been generated by disturbing the pipe by the solenoid which was actuated by the signal generator. The velocity of droplets have been defined by the height of the syringe needle using a traverse. After each experiment, syringe pump was used to fill the ejected volume to the pipe. Rotation of the surfaces have been supplied by a servo motor which can reach 3000 rpm and motor placed onto a 2D traverse system to place the droplets desired position on the test surface. Droplet impact have been recorded at 18000 fps and high lumen non-oscillatory lamp used as light source for the high speed camera. Additionally, to understand the physics of behavior in detail, another high speed camera has been integrated to the setup as slanted. While capturing the slanted views of the drop impact, both cameras have been set 16000 fps and triggered simultaneously.

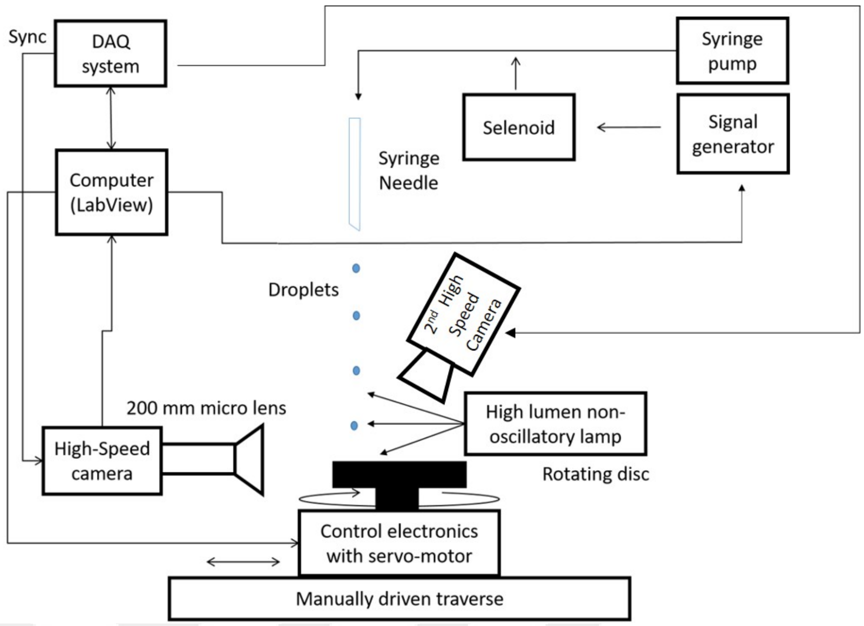


**Figure 3:** Experimental setup

Data acquisition and device control have been made by using LabVIEW software. The components of setup were integrated in a state machine program. First, motor was started. Then, trigger was send to the camera using DAQ to record the video at specified speed. Aftwerwards, another trigger is sent to solenoid to disturb the pipe for droplet generation. After camera recorded specified number of frames, all integrated devices is closed.

## *2.4 Image Calibration and Digital Image Processing Tools*

Image processing has been done by using Matlab and NI Vision softwares. Images have been calibrated by using a calibration plate which has certain size of circle on it. It was used to define the size of unit pixel on image. That size used to calculate the size and velocity of impacted droplets. Droplets have been detected by using a Matlab function which is to find circular objects. Written code (Appendix A.1) takes five sequent frames from a video and detects droplet in the frames and calculates average diameter and velocity to calculate the dimensionless numbers which was used in the analysis. Dynamic contact angle measurements have been done using NI Vision software. In that case, after frames extracted from video using Matlab, all frames imported to NI Vision. Then, edges at the interface have been found by using edge detection comment and angle was measured using caliper. Furthermore, since droplet spreading recording has been done as slanted, it had to be converted top view. The same calibration plate has been used to correct images. Image correction process has been done by using NI Vision software by giving distance of four points on it. The program converts slanted images to the top view images by using given distances (Figure 4). After calibration completed, spreading of the droplet has been measured by using Matlab and NI Vision softwares. Matlab code (Appendix A.2) was written to detect the borders of lamella and measures area, major and minor axis length. However, in some cases because of the reflections Matlab cannot measure size of the lamella properly. Therefore, NI Vision was used to make those measurements using edge detector comment manually frame by frame.

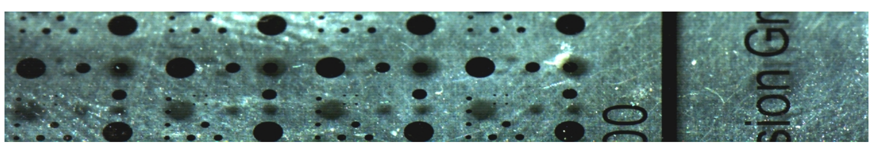

(a)

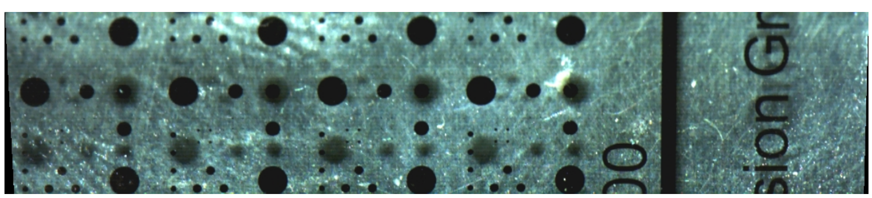

(b)

**Figure 4:** Image correction (a) Slanted view (b) Corrected top view

# CHAPTER III

# SURFACE PREPARATION AND CHARACTERIZATION

Surfaces which have different wettability and roughness prepared to understand the affect on droplet behavior. Hydrophilic, hydrophobic and superhydrophobic surfaces have been prepared as smooth and rough (table 1). Moderate rough case also added to superhydrophobic surface since roughness can be controlled while preparing. Glass used as hydrophilic smooth surface and frosted glass has been used as the rough case. Moreover, paraffin (Parafilm) used to coat the stainless steel plates to make them hydrophobic. In order to obtain the hydrophobic rough surface, parafilm has been applied on the sandpaper. Lastly, superhydrophobic surfaces was obtained by using a surface coating (Ultra-Ever Dry). It was applied by using spin coating technique in which certain amount of coating has been applied while the surface rotating. Roughness of the surface was controlled by the thickness of the bottom layer of the coating. The more applied bottom coating to surface, the rougher became the surface. After the bottom coating applied and dried, top coating was sprayed to the surfaces to make them superhydrophobic and microscope views of coated surfaces can been seen in figure 5.

| Wettability | Hydrophilic | Hydrophobic | Superhydrophobic |
|---|---|---|---|
| Roughness Level - Material | Smooth - Glass | Smooth – Paraffin | Smooth – Ultra-Ever Dry |
| | - | - | Moderate Rough – Ultra-Ever Dry |
| | Rough – Glass | Rough - Paraffin | Rough – Ultra-Ever Dry |

**Table 1:** Test cases

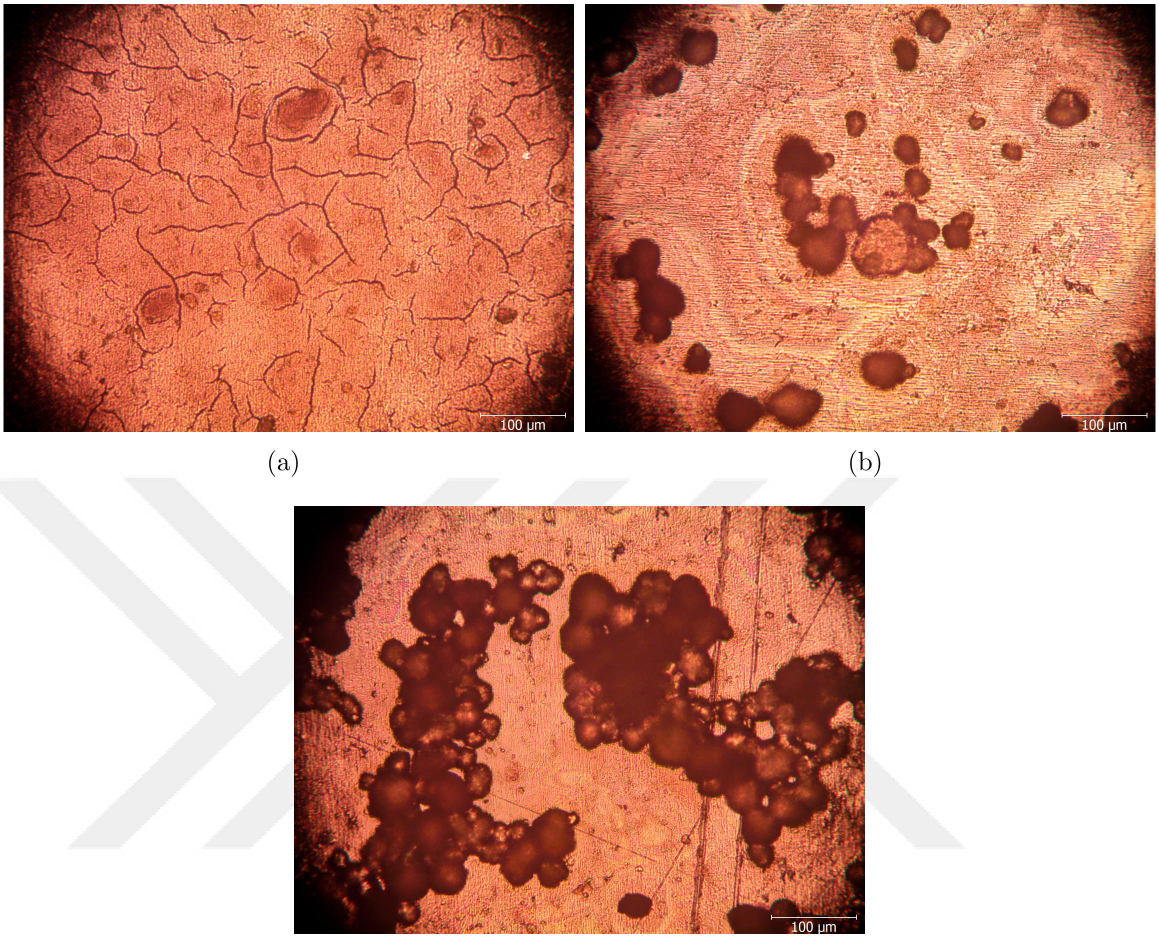


(a) (b) (c)

**Figure 5:** Microscope views of superhydrophobic coating (a) Smooth surface (b) Moderate rough surface (c) Rough surface

## *3.1 Contact Angle Measurements of the Surfaces*

In the experiments, droplet has been deposited on the surface and a frame captured to measure the static contact angle then it is tilted 1 deg/s while recording video at 100 fps until drop slips. Afterwards, the frames which were taken initially and just before the droplet movement analyzed using NI Vision software to measure the contact angles and contact angle values of the test cases can be seen table 2. This experiment has been repeated 10 times for each surface, then average and standard deviation of the measurements have been reported.

| Surface | Material | Roughness level | Advancing CA (º) | Static CA(º) | Receding CA (º) | Hysteresis (ACA-RCA) |
|---|---|---|---|---|---|---|
| **Hydrophilic** | Glass | Smooth | 56.2 ± 4.3 | 54.6±4.1 | 14.0 ± 2.1 | 42.2 |
| | Glass | Rough | 68.5 ± 6.5 | 59.4±5.9 | 17.4 ± 2.4 | 51.1 |
| **Hydrophobic** | Paraffin Coating | Smooth | 112.3 ± 4.1 | 104.2±2.9 | 62.9 ± 2.2 | 49.4 |
| | Paraffin Coating | Rough | 107.6 ± 3.8 | 103.1±4.5 | 67.4 ± 4.1 | 40.2 |
| **Superhydrophobic** | Ultra Ever-Dry Coating | Smooth | 164.1 ± 4.8 | 156.6±4.1 | 145.0 ± 6.5 | 19.1 |
| | Ultra Ever-Dry Coating | Moderate Rough | 160.5 ± 3.6 | 156.2±4.0 | 95.3 ± 8.8 | 65.2 |
| | Ultra Ever-Dry Coating | Rough | 158.2 ± 5.0 | 152.3±4.8 | 135.2 ± 7.3 | 23 |

**Table 2:** Roughness and contact angles for each surfaces

## *3.2 Roughness Measurements of the Surfaces*

Measured data has been filtered by changing the outlier values into average ones and plotted by using Matlab (Figure 6 - 12). 2x2 mm area at the 4 different locations which are close to the impacted regions on the surface have been measured. Average of $R_a$, $R_z$, $R_q$, $R_t$, $S_t$ and impacted droplet diameter are reported in table 3. In the study which has done by Mundo et. al.[4], if $S_t$ is 0.03, surface considered as smooth and if it is 0.86, surface assumed as rough. However, the $S_t$ values of the present study assumed as smooth in their study. The highest $S_t$ of the present study is 0.09 and it is the roughness of the rough superhydrophobic surface.

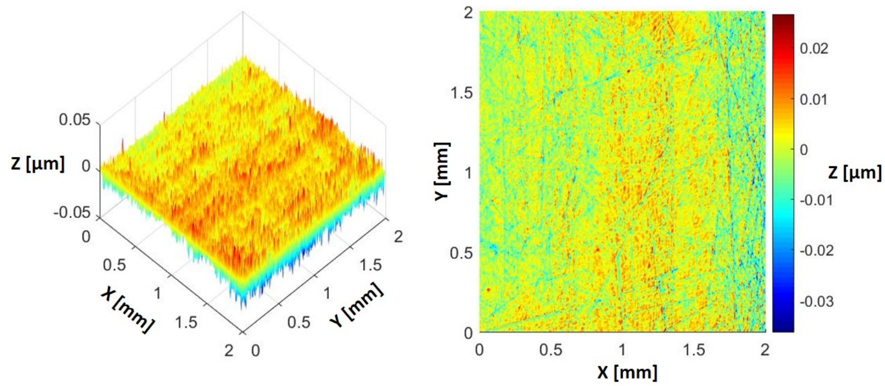


**Figure 6:** Topology of hydrophilic smooth surface

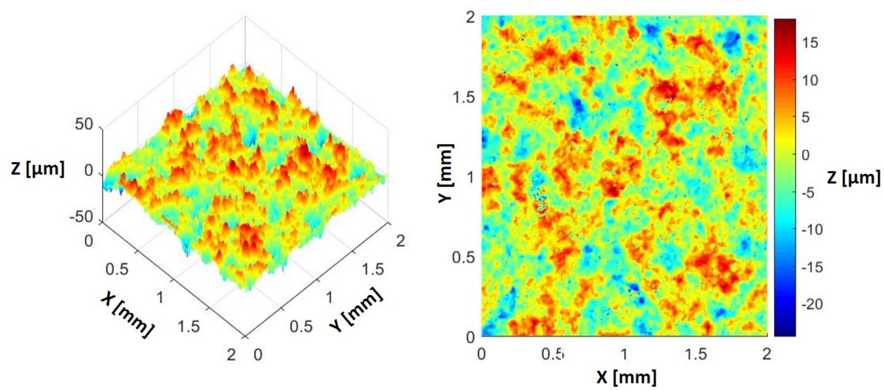


**Figure 7:** Topology of hydrophilic rough surface

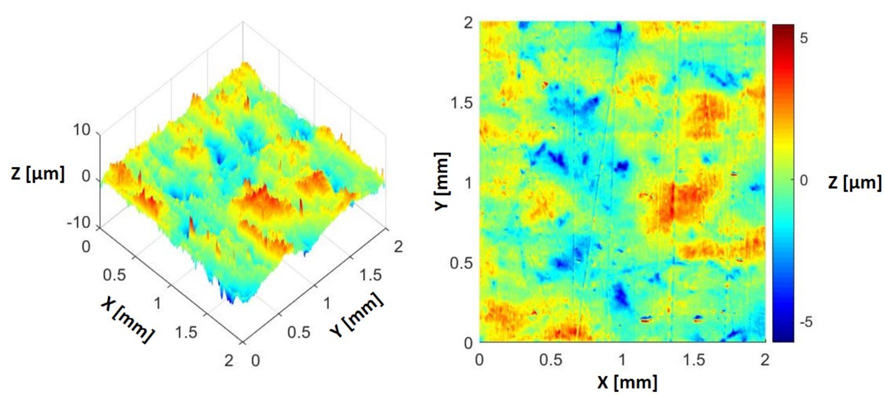


**Figure 8:** Topology of hydrophobic smooth surface

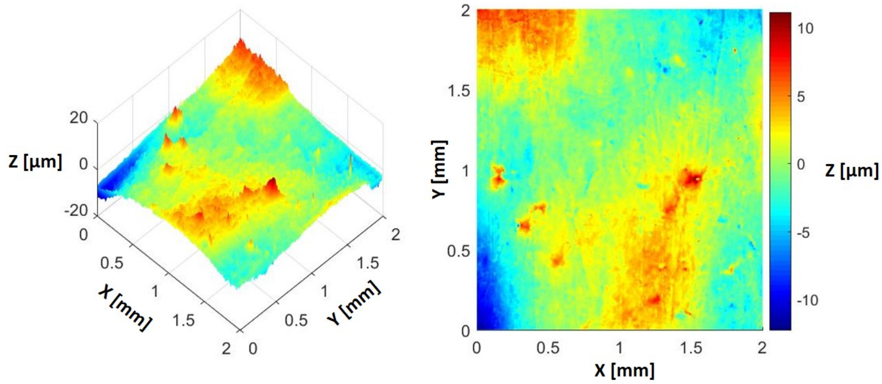


**Figure 9:** Topology of hydrophobic rough surface

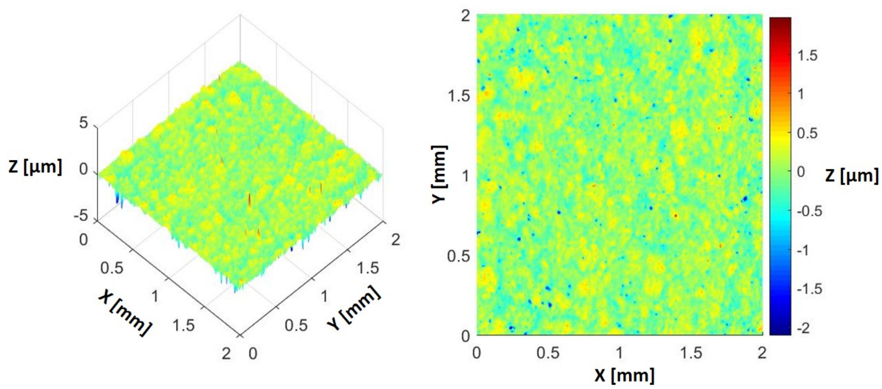


**Figure 10:** Topology of superhydrophobic smooth surface

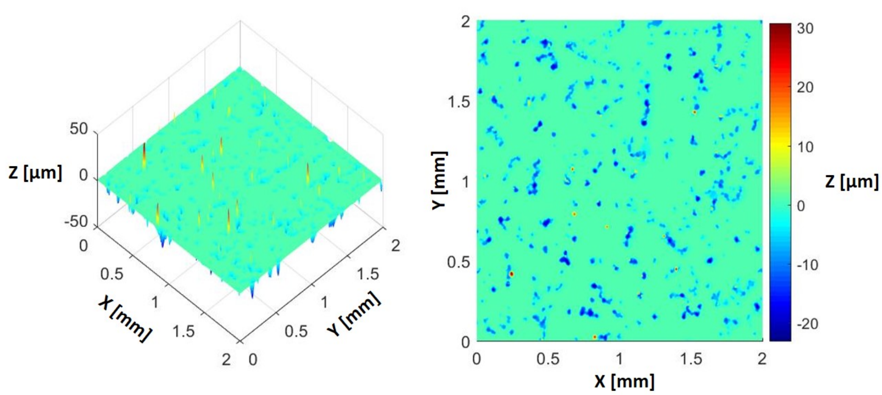


**Figure 11:** Topology of superhydrophobic moderate rough

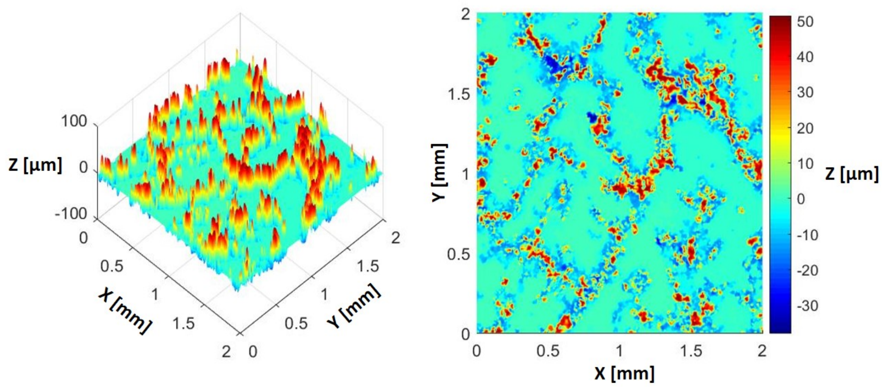


**Figure 12:** Topology of superhydrophobic rough surface

| Surface | Material | Roughness level | $R_a$ (μm) | $R_z$ (μm) | $R_q$ (μm) | $R_t$ (μm) | Droplet Diameter (μm) (mean ± st.dev) | $S_t$ |
|---|---|---|---|---|---|---|---|---|
| **Hydrophilic** | Glass | Smooth | 0.01 | 0.23 | 0.01 | 3.76 | 850.2 ± 223.9 | $4.43 * 10^{-3}$ |
| | Glass | Rough | 4.57 | 90.66 | 5.81 | 53.61 | 806.5 ± 153.8 | $0.07 * 10^{0}$ |
| **Hydrophobic** | Paraffin Coating | Smooth | 0.65 | 13.35 | 1.24 | 12.54 | 856.6 ±207.2 | $0.01 * 10^{0}$ |
| | Paraffin Coating | Rough | 2.31 | 30.13 | 3.10 | 33.39 | 850.5 ± 170.3 | $0.04 * 10^{0}$ |
| **Superhydrophobic** | Ultra Ever-Dry Coating | Smooth | 0.19 | 5.86 | 0.26 | 6.00 | 852.9 ± 223.9 | $7.03 * 10^{-3}$ |
| | Ultra Ever-Dry Coating | Moderate Rough | 1.55 | 56.52 | 3.21 | 58.48 | 881.0 ± 268.3 | $0.07 * 10^{0}$ |
| | Ultra Ever-Dry Coating | Rough | 6.62 | 85.45 | 11.11 | 86.88 | 955.3 ± 275.3 | $0.09 * 10^{0}$ |

**Table 3:** Surface roughness measurements

# CHAPTER IV

# DROPLET IMPACT OUTCOME ON MOVING SURFACES

Regime maps have been created as a function of normal and tangential Weber numbers for each surface and the outcomes upon impact are listed in table 4 and described in the following text.

| Superhydrophobic | | | Hydrophobic | | Hydrophilic | |
|---|---|---|---|---|---|---|
| **Smooth** | **Moderate Rough** | **Rough** | **Smooth** | **Rough** | **Smooth** | **Rough** |
| Rebound | Rebound | Rebound | Deposition | Deposition | Deposition | Deposition |
| Rebound with Vertical Split | Rebound with Leading Edge Split-Splashing | Rebound with Leading Edge Split-Splashing | Split Deposition | Split Deposition | Deposition with Trailing Edge Droplet Formation | Deposition with Trailing Edge Droplet Formation |
| Rebound with Leading Edge Split | Rebound with Both Sides Split-Splashing | Rebound with Both Sides Split-Splashing | Deposition with Trailing Edge Split | Deposition with Trailing Edge Split | Deposition with Trailing Edge Split | Deposition with Trailing Edge Split |
| Rebound with Both Sides Split | Rebound with Receding Breakup-Splashing | Rebound with Receding Breakup-Splashing | Deposition with Vertical Split | | | |

**Table 4:** Observed droplet impact outcomes on moving surfaces

## *4.1 Drop Impact Outcome on Superhydrophobic Surfaces*

Rebound with vertical split, rebound, rebound with the leading edge split, rebound with receding breakup and rebound with both sides split have been observed in the experiments. Also, splashing may be observed depending on the roughness levels of the test cases.

**Rebound with Vertical Split:** Droplet hits to the stationary surface and lamella expands symmetrically over the surface. Then, it creates upward jet and due to instability at the jet, some part of the drop splits while rest of the droplet also rebounds from surface (Figure 13). This happens when $We_t$ is very low.

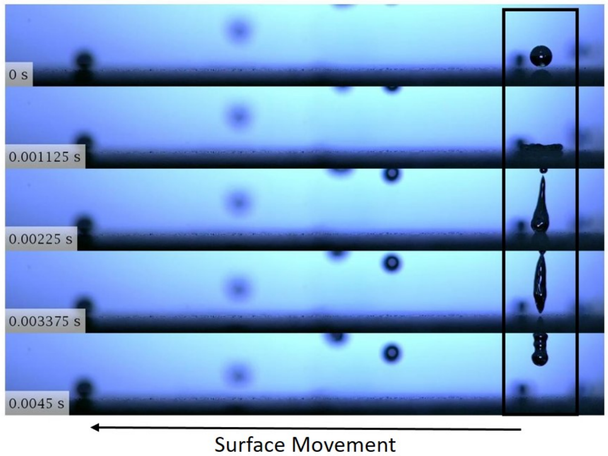


(a)

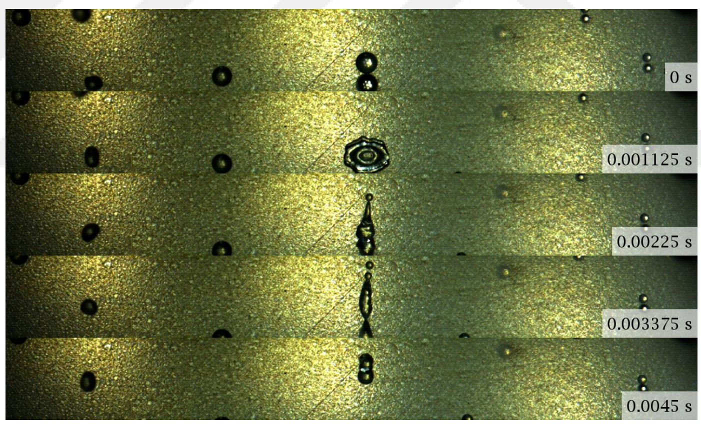


(b)

**Figure 13:** Rebound with vertical split on superhydrophobic smooth surface ($We_t$= 0, $We_n$= 55.40); (a) Side view, (b) Slanted view

**Rebound:** Droplet hits to surface and creates ellipse shape rim in the spreading phase. Then, both side of the rim impact each other starting from the leading edge in the receding phase. Since rim at the leading edge collides first, rebound starts from leading edge and goes to trailing edge of the drop. At the end, droplet rebounds as completely distorted (Figure 14).

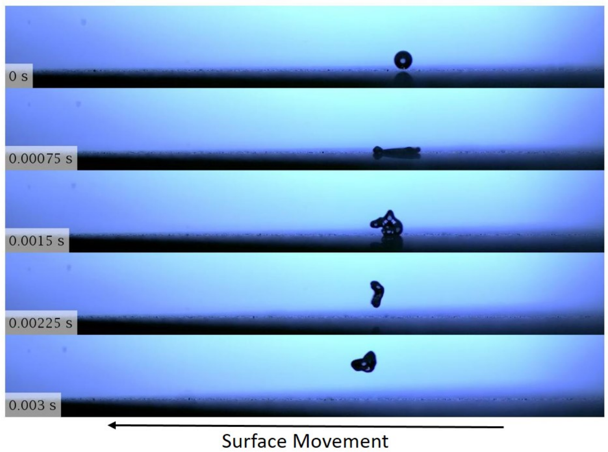


(a)

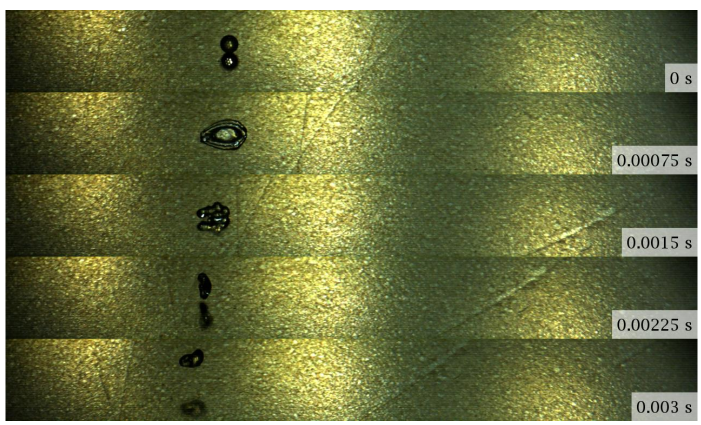


(b)

**Figure 14:** Rebound on superhydrophobic smooth surface ($We_t$= 201.56, $We_n$= 33.47); (a) Side view, (b) Slanted view

**Rebound with Receding Breakup:** Droplet hits to the surface and creates lamella with the finger formation in the spreading phase. Then, it starts to recede and splitting is seen at the necking areas. Afterwards, rest of the droplet rebounds from the surface (Figure 15).

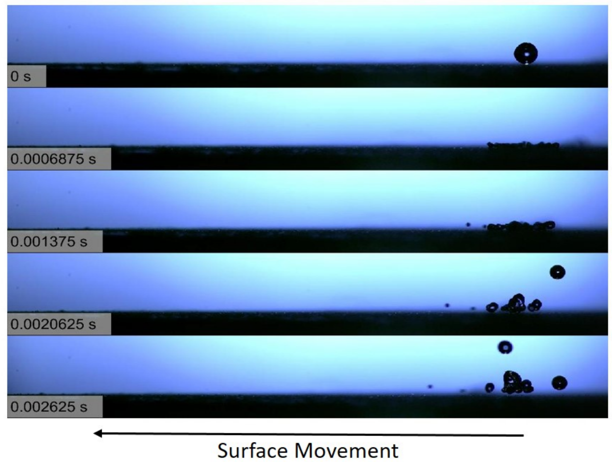


(a)

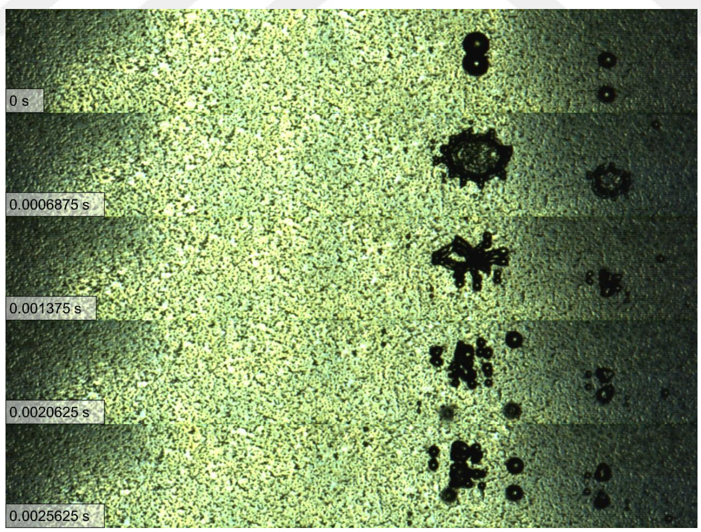


(b)

**Figure 15:** Rebound with receding breakup on superhydrophobic moderate rough surface ($We_t$= 18.54, $We_n$= 129.67); (a) Side view, (b) Slanted view

**Rebound with Leading Edge Split:** Upon impact, droplet forms an ellipse shape lamella in the spreading phase. Then, starting from the leading edge, it starts to recede radially and propagates to the trailing edge. It recedes until the major axis length of the ellipse reaches to zero so both side of the rim impacts to each other and forms ligament. Then, rim impact creates lift off and instabilities at the ligament causes splitting at the leading edge (Figure 16).

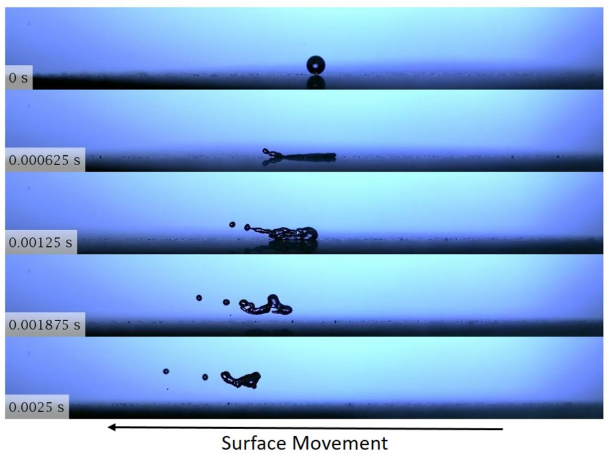


(a)

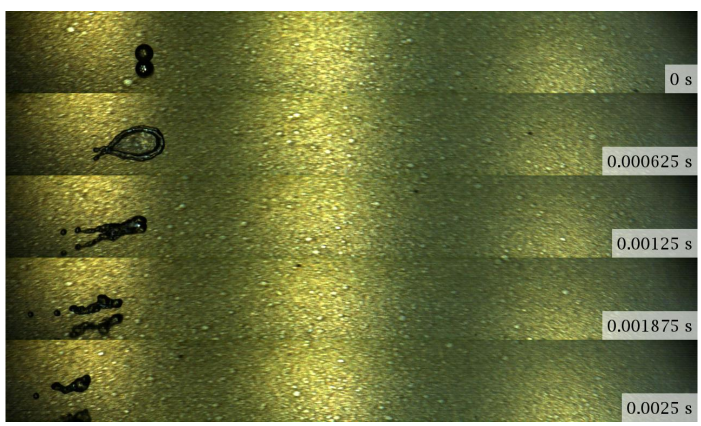


(b)

**Figure 16:** Rebound with leading edge split on superhydrophobic smooth surface ($We_t$= 535.30, $We_n$= 57.29); (a) Side view, (b) Slanted view

**Rebound with Both Sides Split:** After impact to the surface droplet creates ellipse shape lamella due surface movement. Receding starts from the leading edge of the lamella and it continues until two side of the ellipse shape rim impacts each other. Afterwards, created ligament lifts off and splits same as the rebound with leading edge split behavior. On the other edge of the droplet, lamella forms fingering while spreading and droplets split around the rim in the receding phase. At the end, all splitted and rest of the droplet rebounds from the surface. Hence, leading and trailing edge of the drop behaves differently in this case[5]. It is the combination of receding breakup and leading edge split at the trailing and leading edge of the droplet, respectively (Figure 17).

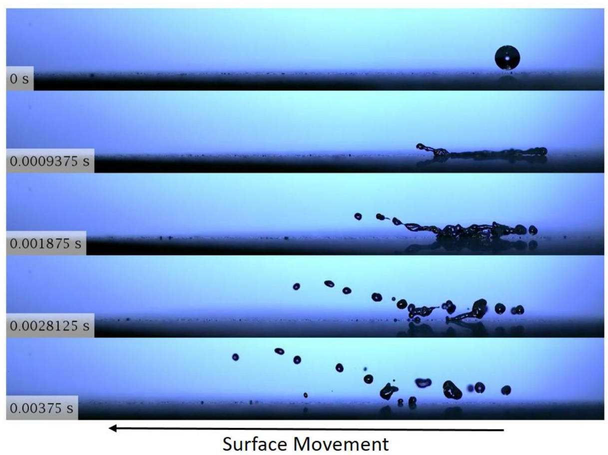


(a)

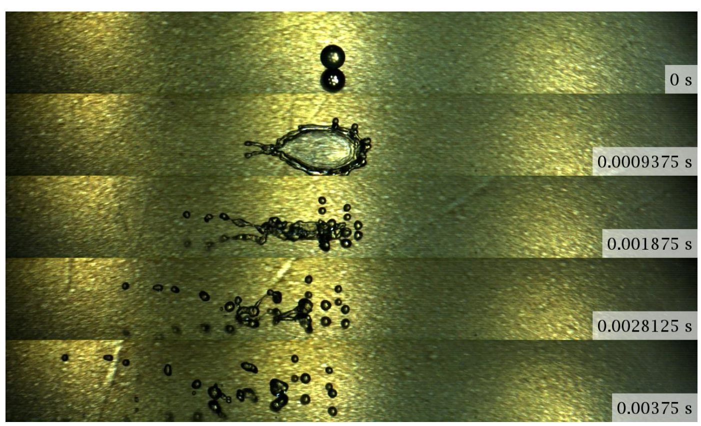


(b)

**Figure 17:** Rebound with both sides split on superhydrophobic smooth surface ($We_t$= 726.21, $We_n$= 94.50); (a) Side view, (b) Slanted view

### 4.1.1 Regimes in Superhydrophobic Smooth Surface

Rebound with vertical split, rebound, rebound with leading edge split and rebound with both sides split can be seen on the superhydrophobic smooth surface (Figure 18).

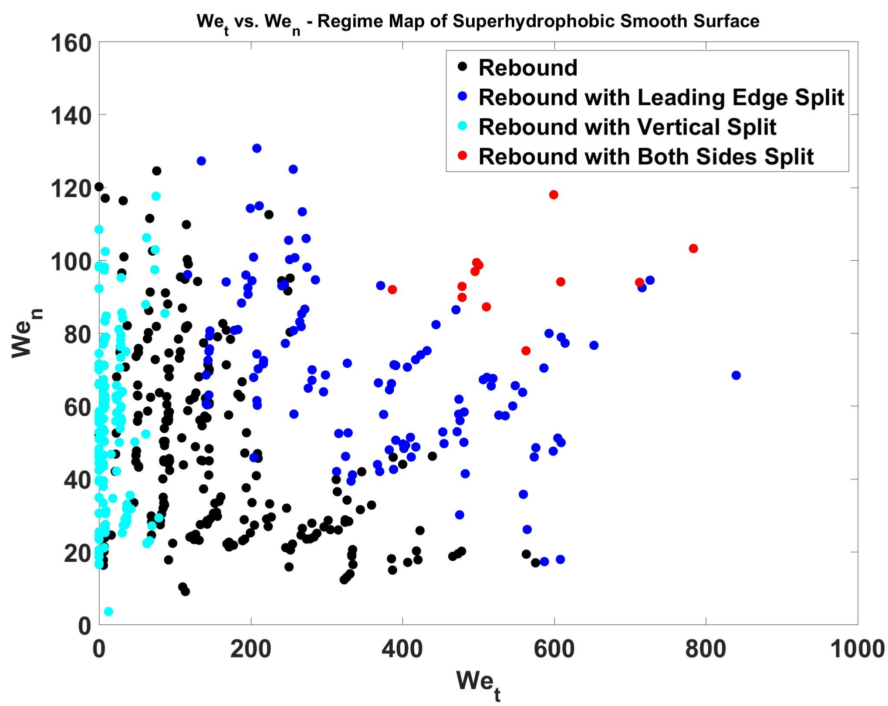


**Figure 18:** Regime map of superhydrophobic smooth surface

Rebound with vertical split is seen at the low tangential Weber number because droplet is not exposed to significant shear. Kinetic energy which the droplet has prior to impact cannot be dissipated at the spreading phase. Then droplet creates an upward jet and splitting have been observed due to instability at the jet and rest of the drop rebounds from the surface as well. But when tangential Weber number is increased, the tangential spreading of the lemalla increases. Therefore it cannot create upward jet and vertical splitting is suppressed and droplet rebounds. Moreover, when tangential and normal Weber number increased, splitting is seen at the leading edge because of the surface movement. It causes increase in the tangential spreading of the lamella. Shape of the lamella turns into ellipse in the spreading phase.

Then, rim recedes until it turns into ligament and it lifts off. Due intabilities in the ligament, splitting is seen at the leading edge. Lastly, when $We_n$ is increased more at high $We_t$, spreading increases in radial and tangential directions. After formation of fingering around the lamella, splitting is observed at the trailing edge (receding breakup). Likewise, due to increase in the $We_t$, ligament is formed and lifted off from the surface. Splitting is seen because of the instability of ligament created at the leading edge. In addition, regime conflict areas can be seen in some parts of the regime map, this is due to high sensitivity on surface homogeneity in roughness and contact angle.

### 4.1.2 Regimes in Superhydrophobic Moderate Rough Surface

The regime map for the superhydrophobic moderate rough is shown in figure 19. Rebound, rebound with leading edge split, rebound with both sides split and rebound with receding breakup which were shown in the previous case have been observed in the superhydrophobic moderate rough case. However, contact angle hysteresis of this surface is higher than the other surperhydrophobic surfaces (see table 2). This means that while spreading on the surface it will behave like smooth surface but effect of the receding contact angle will be seen in the retraction phase.

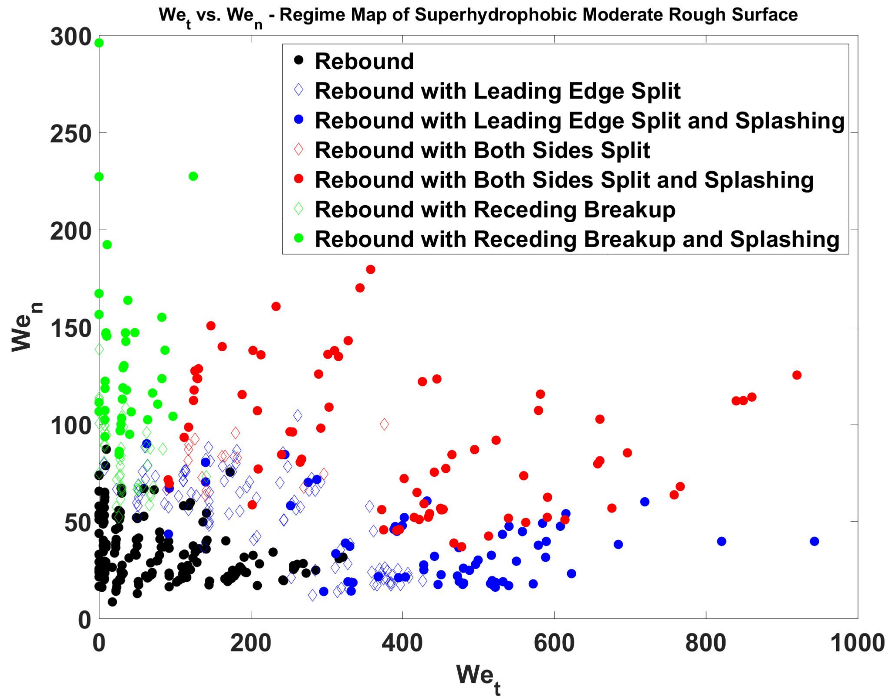


**Figure 19:** Regime map of superhydrophobic moderate rough surface

It can be seen from the figure 19, rebound is seen at the lower $We_n$ and $We_t$ when compared to the smooth surface. When $We_n$ increases at low $We_t$, fingers started to be seen around the rim and they split from the rim while receding and rebounding (rebound with receding breakup). If $We_n$ rises more, splashing occurs around the rim because of the roughness. Likewise, increase in $We_t$ triggers splashing phenomena. Furthermore, rebound with leading edge split is seen at the higher $We_t$ values but at much lower $We_n$ than the smooth case. In this case droplet is elongated by the surface motion in the spreading phase due to low receding contact angle. Moreover, rebound with both sides split is seen at high $We_n$ and $We_t$. Both ends of lamella behave different; splitting is seen at the leading edge due to surface movement, whereas receding breakup is observed at the trailing edge due to drop inertia. Rest of the impacted drop rebounds from the surface as many splitted droplets.

### 4.1.3 Regimes in Superhydrophobic Rough Surface

Regime map for this case is shown in figure 20. It is seen that rebound is observed at the low $We_n$ and $We_t$ values and even for very small $We_n$ values surface tension of the drop prevents split. Rebound is not observed much when it is compared with the moderate rough case because of the roughness difference. Similar to the moderate rough case, rebound with receding breakup with and without splashing is seen at $We_n > 50$ and $We_t < 100$. Since tangential Weber number is low in this case ,it spreads on the surface with fingering around the rim and splitting is seen while receding. Likewise, when $We_t$ increases at low $We_n$, rebound with leading edge split and splashing are seen. Since the surface is rougher than the others, splashing phenomena is seen at the lower $We_n$ and $We_t$ values. The other obvious difference for this case is , rebound with both sides split and splashing can be seen at much lower $We_n$ and $We_t$ values. The results clearly show that roughness level plays a crucial role of the droplet behavior on the superhydrophobic surfaces.

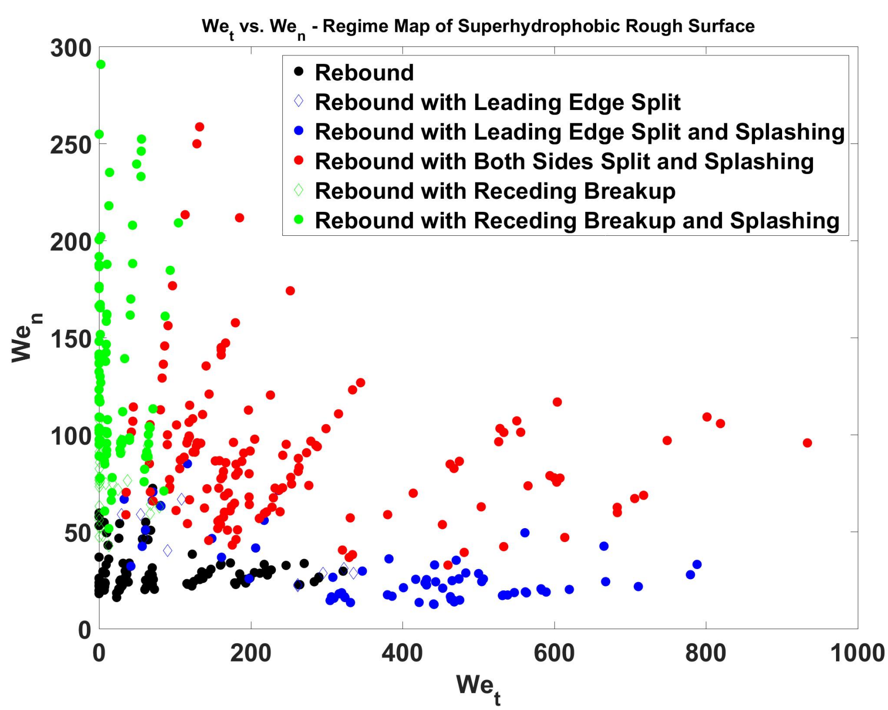


**Figure 20:** Regime map of superhydrophobic rough surface

## 4.2 Drop Impact Outcome on Hydrophobic Surfaces

Deposition with vertical split, deposition, split deposition and split deposition with trailing edge split are the observed outcomes from drop impact on hydrophobic surfaces.

**Deposition with Vertical Split:** Droplet hits to surface and creates symmetric lamella in the spreading phase. Then, it recedes and creates upward jet due to high velocity of the lamella. After necking, split of jet in the vertical direction is observed (Figure 21).

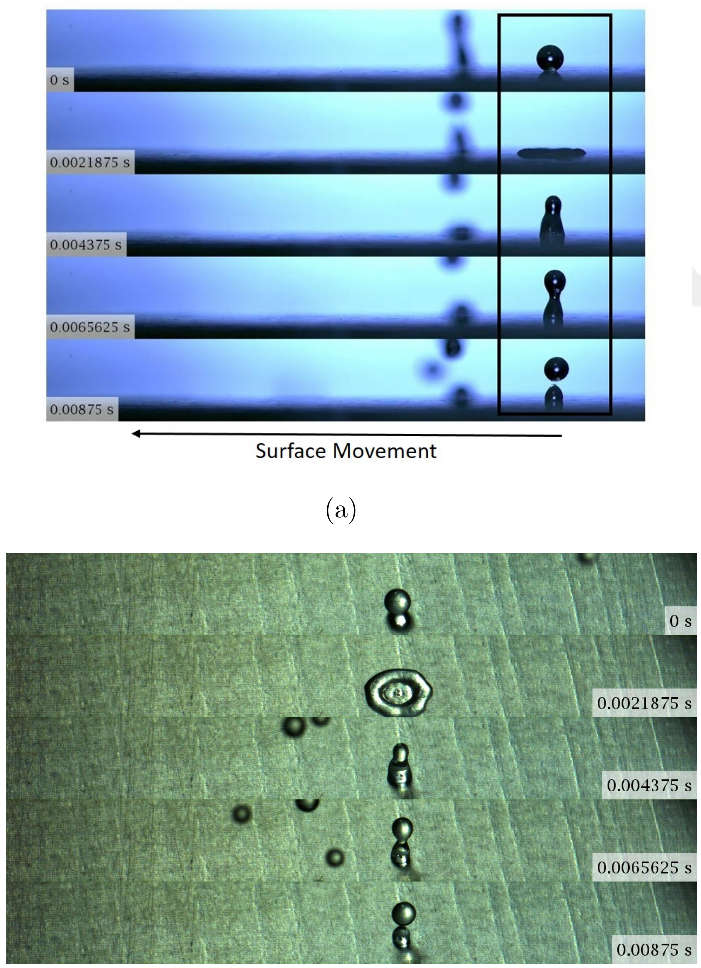


(a)

(b)

**Figure 21:** Deposition with vertical split on hydrophobic smooth surface ($We_t$= 0, $We_n$= 104.29); (a) Side view, (b) Slanted view

**Deposition:** Droplet hits to surface and creates symmetric lamella in the spreading phase. Then it recedes and stay on the surface as a truncated sphere (Figure 22).

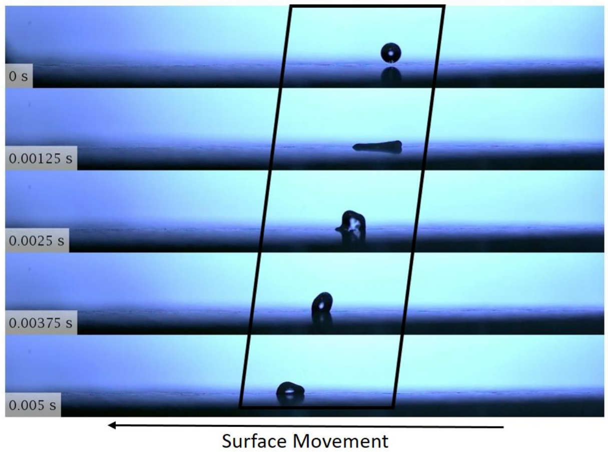


(a)

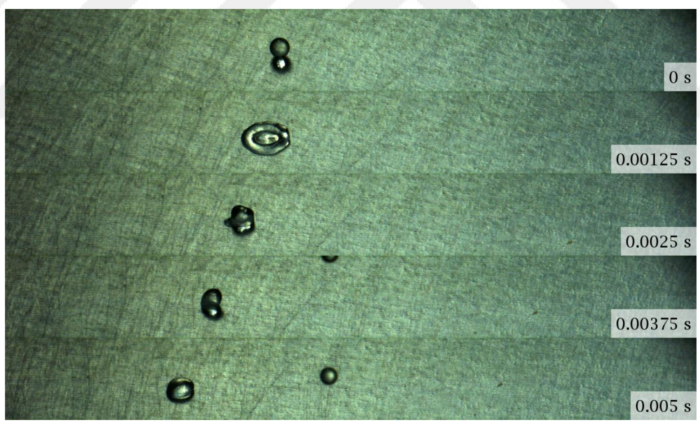


(b)

**Figure 22:** Deposition on hydrophobic smooth surface ($We_t$= 16.16, $We_n$= 45.52); (a) Side view, (b) Slanted view

**Split Deposition:** Droplet hits to surface and spreads as ellipse shape due to tangential velocity. Then, minor axis length of the ellipse starts to decrease until it reaches zero, so that rims impact each other in the receding phase and it turns into ligament and splits on the surface (Figure 23).

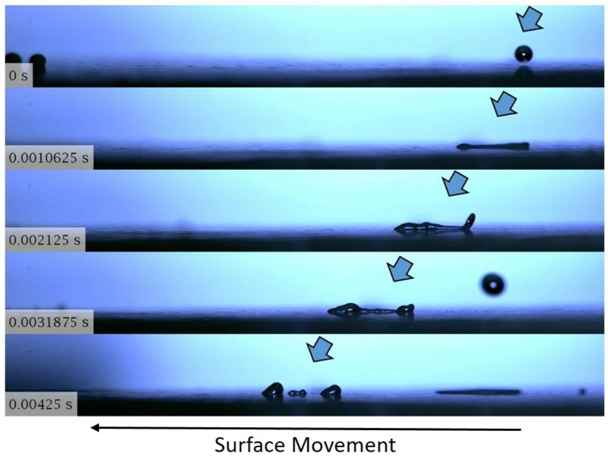


(a)

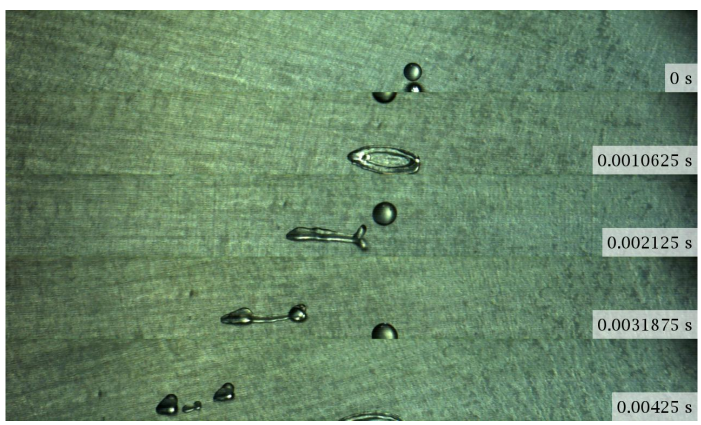


(b)

**Figure 23:** Split deposition on hydrophobic smooth surface ($We_t$= 114.68, $We_n$= 43.65); (a) Side view, (b) Slanted view

**Deposition with Trailing Edge Split:** Droplet hits and spreads over the surface but tangential spreading of lamella increases too much in the spreading phase due to high $We_t$. Then, length of the lamella decreases in the radial direction in receding phase and rims collide each other. Trailing edge of the ligaments lifts off due to high $We_t$. Then, droplet splits from the trailing edge (Figure 24).

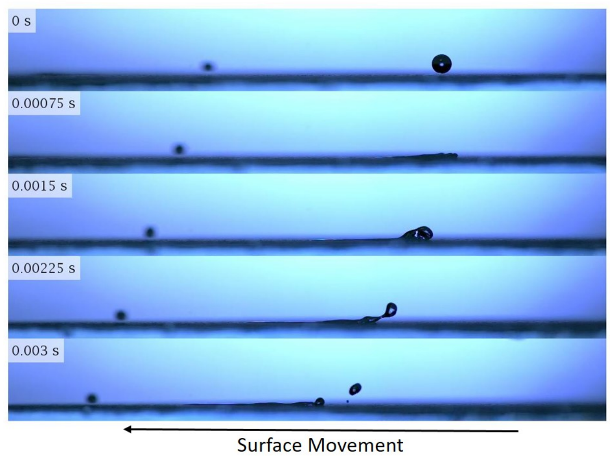


(a)

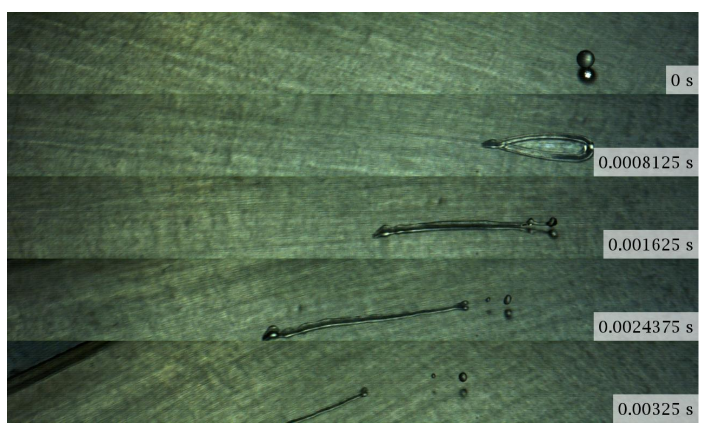


(b)

**Figure 24:** Deposition with trailing edge split on hydrophobic smooth surface ($We_t$= 530.95, $We_n$= 43.91); (a) Side view , (b) Slanted view

### 4.2.1 Regimes in Hydrophobic Smooth Surface

Outcomes of drop impact of the hydrophobic smooth surface is shown in figure 25. Deposition with vertical split is seen at the stationary surface ($We_t$=0). However, when $We_t$ is increased, vertical splitting will be inhibited, because droplet spreading on the surface, surface movement causes asymmetric spreading over the surface and it cannot create upward jet and consequently it deposits. If $We_t$ increases more, droplet splits on the surface due to rim impact and it deposits (split deposition). More increase in the $We_t$ causes edge splitting from the tail of droplet and splitted part lifts off from the surface, while the other part of droplet deposits on the surface.

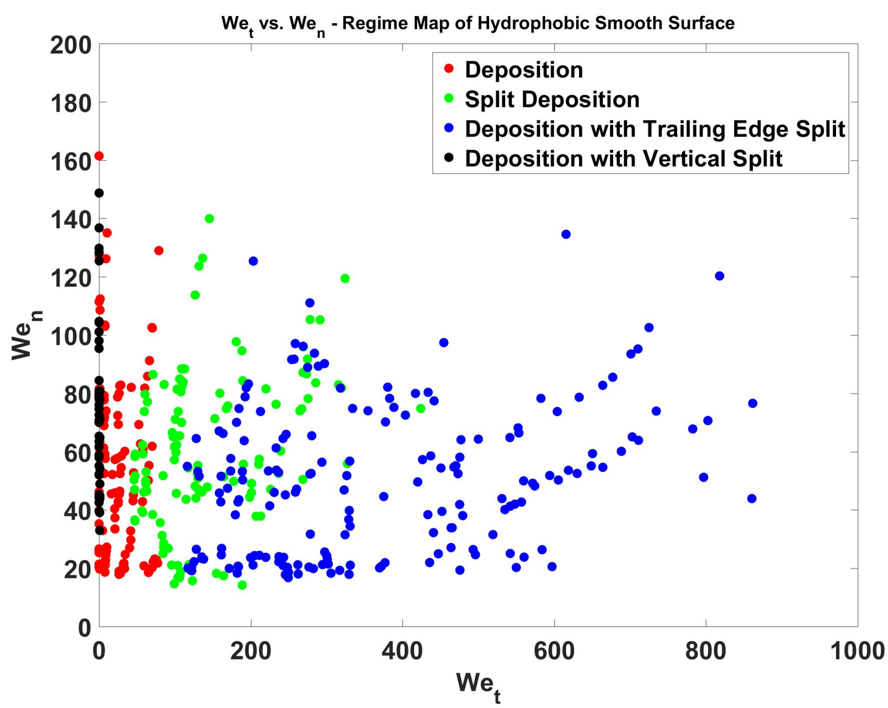


**Figure 25:** Regime map of hydrophobic smooth surface

### 4.2.2 Regimes in Hydrophobic Rough Surface

The regime map of the hydrophobic rough surface is shown figure 26. Roughness of the surface increased energy dissipation so that deposition with vertical split cannot be observed. It is observed that droplets deposit on the surface at lower $We_t$ when compared to that of smooth surface. When the tangential velocity of the surface increases droplets start to split and deposit (split deposition) on the surface. If the tangential velocity increases furthermore, between $We_t$= 150 and $We_t$=300 both split deposition and split deposition with trailing edge split can be seen. It is seen from the figure 26 that in some cases one or the other behavior can be seen even for very close data points.The width of the transition is most probably dependent on the homogeneity of surface properties. For $We_t > 350$, solely deposition with trailing edge split can be observed.

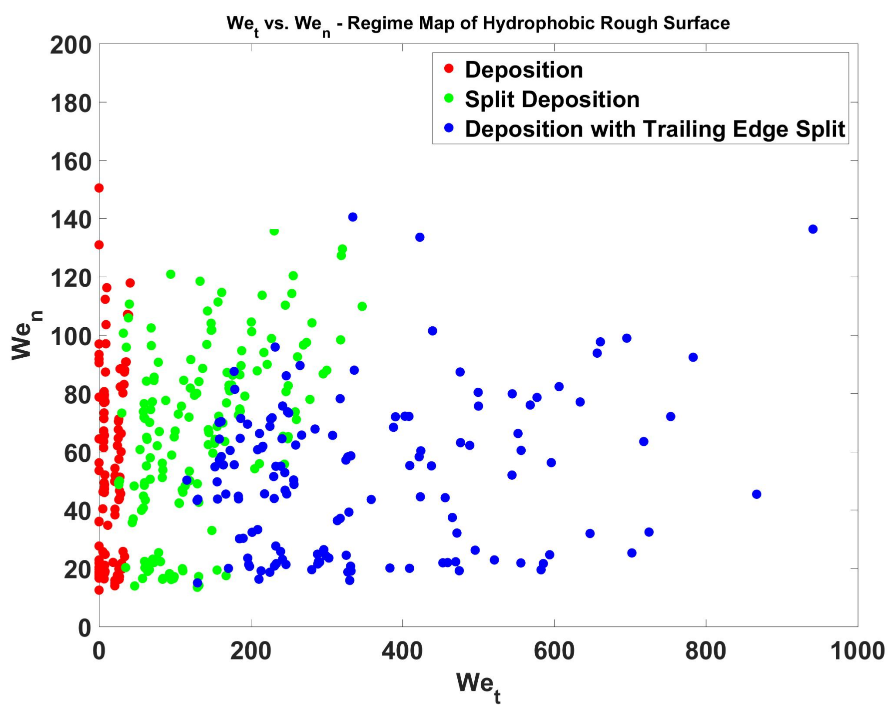


**Figure 26:** Regime map of hydrophobic rough surface

## 4.3 Drop Impact Outcome on Hydrophilic Surface

Drop impacts on hydrophilic smooth and rough surfaces result in deposition, deposition with wake formation and deposition with trailing edge split have been observed in the experiments.

**Deposition:** Droplet hits to surface and creates symmetric lamella in the spreading phase. Then it recedes and stays on the surface as a truncated sphere (similar to hydrophobic case figure 22).

**Deposition with Trailing Edge Droplet Formation:** Droplet spreads over the surface by creating ellipse shape lamella, due to surface movement. At the trailing edge, spreading is suppressed due to surface motion. However, radius of curvature of the droplet is a lot smaller at the trailing edge, which results in earlier receding and collision of two sides of rim and droplet formation. If $We_t$ is high enough, wave formation can be seen at the trailing edge. When lamella reaches to the maximum spreading, it turns into film on the surface and it cannot recede much because of the low receding contact angle (Figure 27).

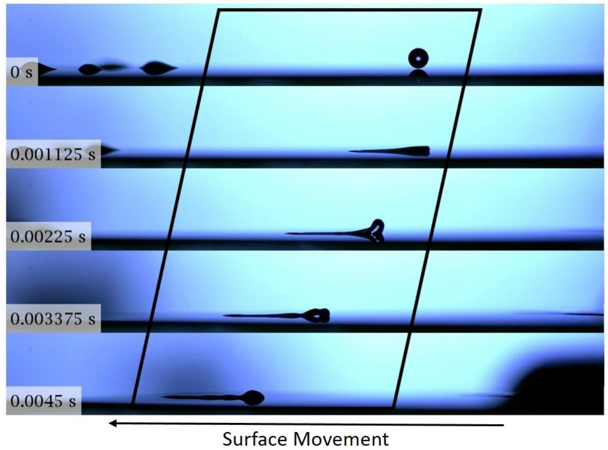


(a)

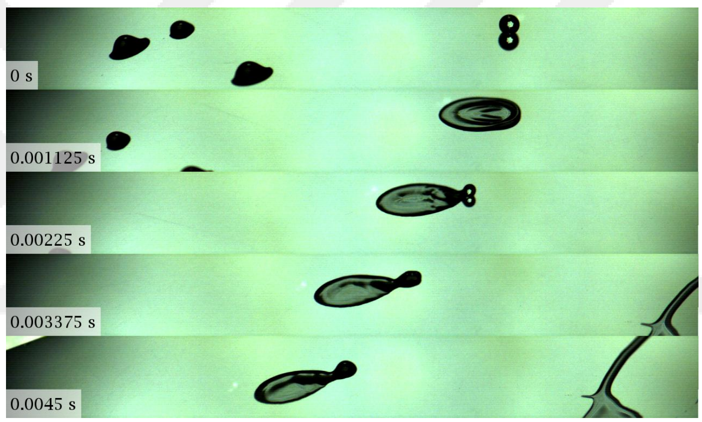


(b)

**Figure 27:** Deposition with trailing edge droplet formation on hydrophilic smooth surface ($We_t$= 67.42 , $We_n$= 49.32); (a) Side view, (b) Slanted view

**Deposition with Trailing Edge Split:** Similar to the previous outcome, drop hits and spreads over the surface as ellipse due to high $We_t$ at the spreading phase. Then, rim of the lamella starts to recede and collision of two side of rim is seen. As the rim is merged, some part of the trailing edge lifts off from the surface and splits. (Figure 28).

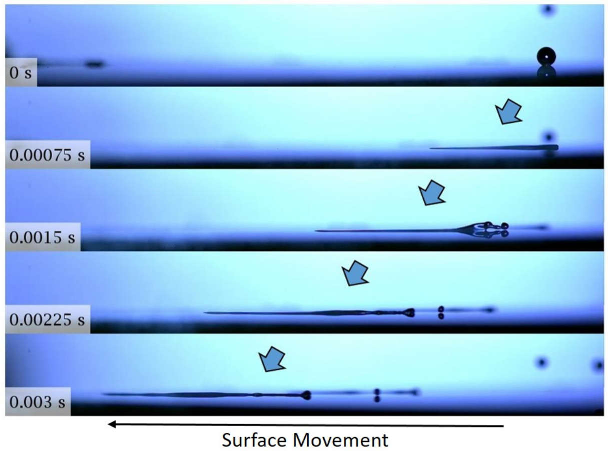


(a)

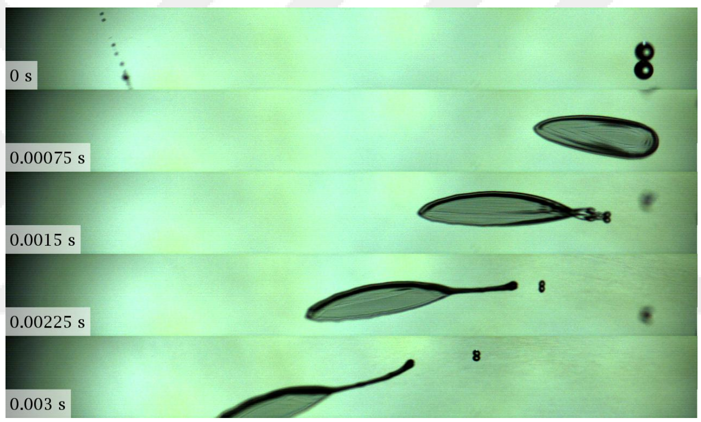


(b)

**Figure 28:** Deposition with trailing edge split on hydrophilic smooth surface ($We_t$= 574.14 , $We_n$= 91.09); (a) Side view, (b) Slanted view

### 4.3.1 Regimes in Hydrophilic Smooth Surface

Regime map of the observed behaviors can be found figure 29. At low $We_t$ numbers which is between 0-50, droplet hits and deposits on the surface. Also, when $We_t$ is increased to 70, it starts to elongate on the surface with wake formation due to surface motion and this behavior is seen until tangential Weber number reaches to 300. After this threshold, more increase in the $We_t$ causes splitting at the trailing edge and rest of the droplet elongates on the surface.

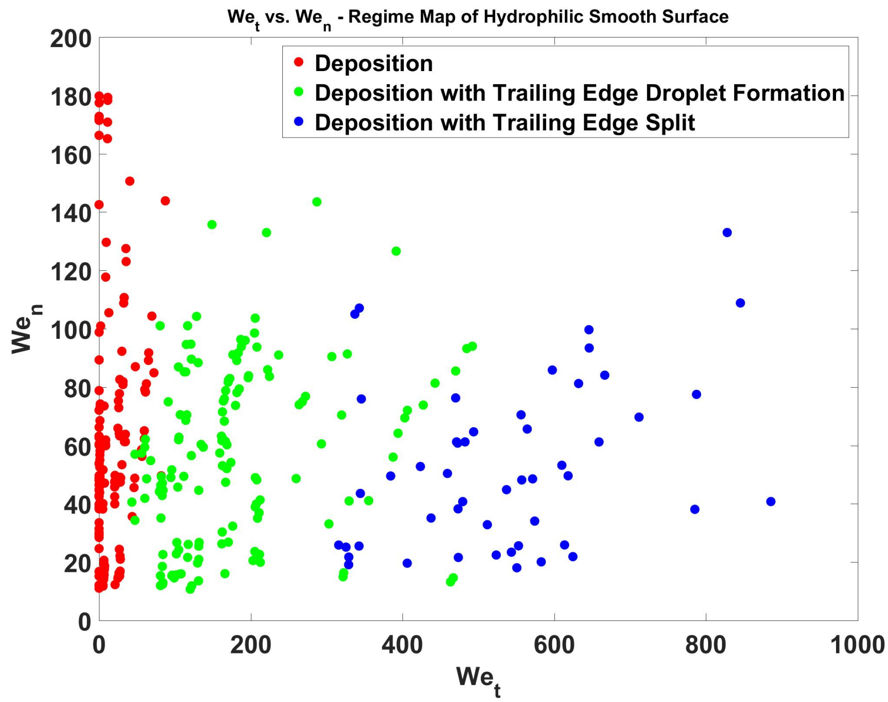


**Figure 29:** Regime map of hydrophilic smooth surface

### 4.3.2 Regimes in Hydrophilic Rough Surface

The regime map for the hydrophilic rough surface can be seen figure 30. At low $We_t$, droplets deposit on the hydrophilic rough surface but when $We_t$ increases, droplet starts to elongate on the surface with the formation of wake at the trailing edge because of the pulling effect of the surface movement but this can be observed in the regime map over a very limited range of $We_n$ numbers. Afterwards, it starts to split from the trailing edge while the rest is depositing on the surface when $We_t$ is increased. The roughness of surface causes earlier drop splitting at the trailing edge when it is compared with the smooth case.

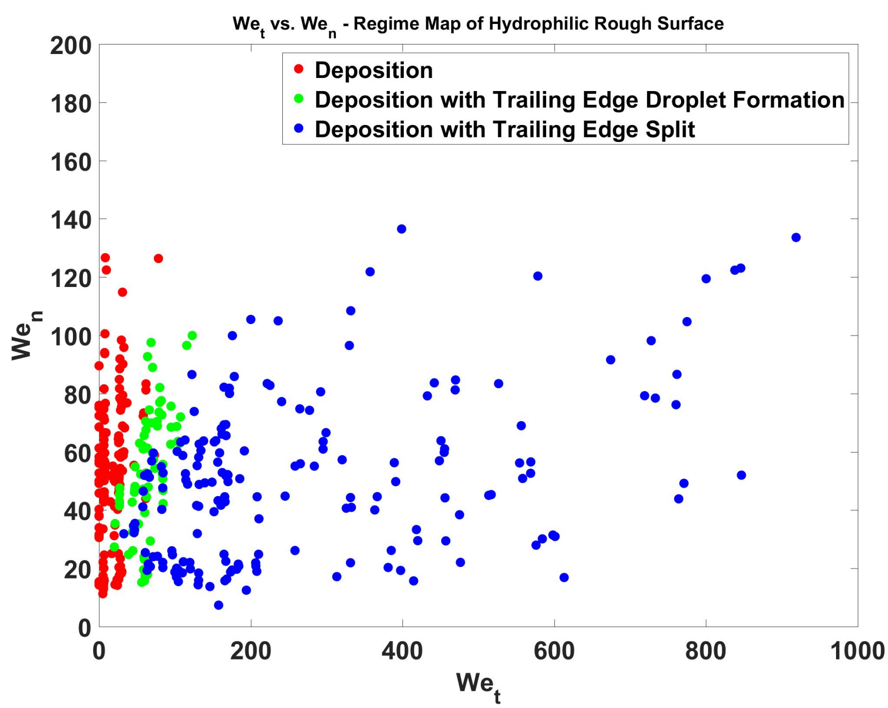


**Figure 30:** Regime map of hydrophilic rough surface

# CHAPTER V

# DROPLET SPREADING ON MOVING SURFACES

Droplet spreading on moving smooth hydrophobic and hydrophilic surfaces have been studied by changing $We_n$ and $We_t$. Time evolution of droplet spreading has been visualized and quantified. Radial, tangential and area spread factor have been measured from the frames and plotted with respect to nondimensional time. Radial spread factor calculated as spreading at the radial direction over initial droplet diameter. Tangential spread factor is the ratio of spreading at the tangential direction and initial droplet diameter (Figure 31). Area spread factor can be found by multiplying these nondimensional numbers. Nondimensional time is calculated by multiplying time with initial droplet velocity over initial droplet diameter.

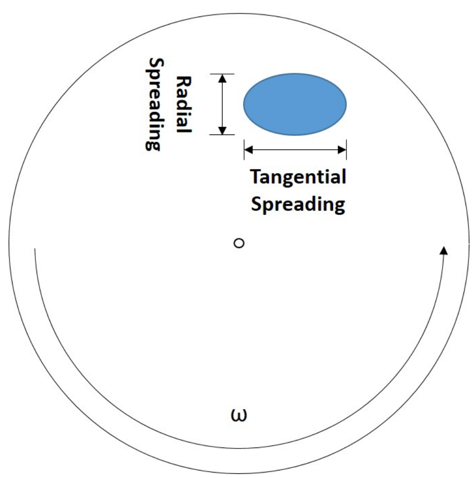


**Figure 31:** Definition of radial and tangential spreading on rotating surface

Droplet spreading on moving surfaces can be separated into three phases. These are advancing, receding and equilibrium phases. After impact, droplet creates ellipse shape lamella due to surface movement and it spreads until lamella reaches maximum spreading. This is called as advancing phase. When it reached to the maximum spreading, it takes some time to convert advancing to receding contact angle and it is called pinning time. This depends on the hysteresis and receding contact angle of the surface[5]. Then, lamella starts to recede depending on the receding contact angle. If the receding contact angle of the surface is small, it cannot recede much. However, if it is high, it can recede even both side of the lamella impact each other. After it consumed all the energy supplied by droplet intertia, it can stay on the surface depending on $We_t$ or due to centrifugal force effect it moves radially outward (Equilibrium phase). Droplet spreading on hydrophobic and hydrophilic surfaces can be seen Figure 32 and details of the spreading will be explained in following sections.

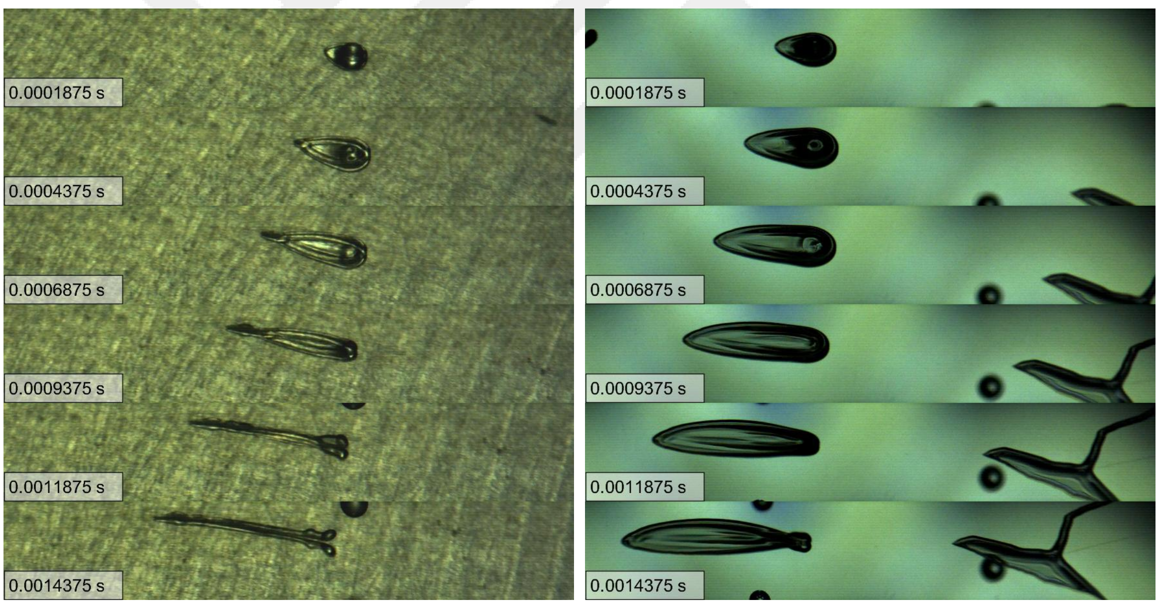


(a) (b)

**Figure 32:** Spreading on (a) hydrophobic and (b) hydrophilic surfaces

## *5.1 Droplet Spreading on Moving Hydrophobic Smooth Surface*

After drop impacted in the advancing phase, droplet spreads over the surface and creates lamella with rim. Shape of it depends on the surface movement. If $We_t$ is high, it starts to elongate in tangential direction and forms ellipse shape. After it reached to maximum spreading at the radial direction, receding starts and recedes until both sides of the rim impact each other. On the other hand, if $We_t$ is small, it spreads and recedes similar to stationary surface case. At the equilibrium phase, droplet can stay on the surface since all the energy consumed. It can also move radially outward due to centrifugal force created by rotation. Effect of $We_n$ and $We_t$ have been examined on radial, tangential and area spread factor. In the study, effect of $We_n$ and $We_t$ on spreading has been investigated on hydrophobic surface. First, effect $We_n$ is observed while $We_t$ kept constant at low, moderate and high level. Then influence of $We_t$ is investigated while $We_n$ kept constant at low, moderate and high. Spreading analysis started just after droplet hits to surface and finished until any reflection or splitting is observed at the image. Therefore, droplet spreading cannot be presented as full cycle for the cases but advancing and some part of the receding phase of the spreading was measured for all cases.

### 5.1.1 Effect of $We_n$ on Spreading for Hydrophobic Smooth Surface

#### *5.1.1.1 Effect of $We_n$ on Radial Spread Factor at Low, Moderate and High $We_t$*

Radial spread factor as a function of $We_n$ at low, moderate and high $We_t$ has been studied (Figure 33). It is found out that, when $We_n$ increased, radial spread factor of droplet increases at low, moderate and high $We_t$. Also, as $We_n$ increases, it takes more time to reach maximum radial spreading on the surface at low and moderate $We_t$ cases.

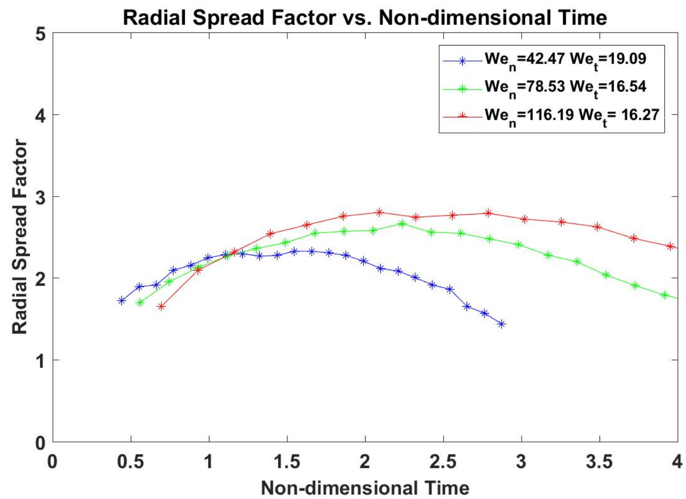


(a)

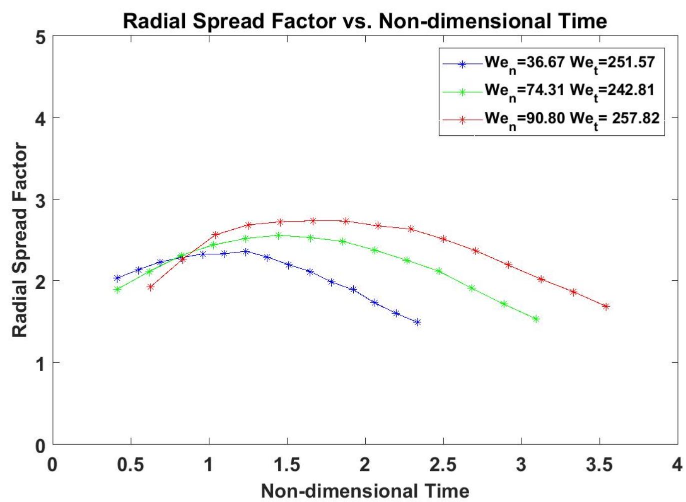


(b)

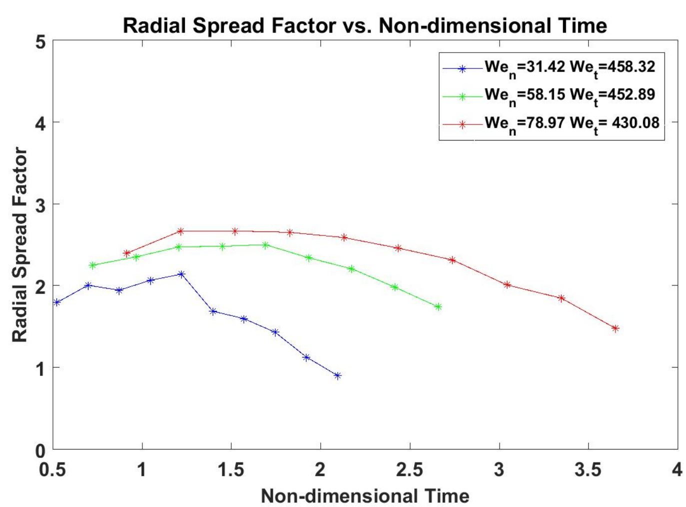


(c)

**Figure 33:** Effect of $We_n$ on radial spread factor for hydrophobic surface

#### 5.1.1.2 Effect of $We_n$ on Tangential Spread Factor at low, Moderate and High $We_t$

Effect of $We_n$ onto tangential spreading at different $We_t$ is shown at figure 34. It is seen that tangential spreading shows similar tendency with radial spreading at low $We_t$. Since surface movement does not affect lamella much, as $We_n$ increases, spreading rises in all directions. However, when $We_t$ reached to moderate and high, tangential spread factor rises as $We_n$ reduces so they are inversely proportional. When maximum tangential spread factor examined, it is mostly depend on $We_t$.

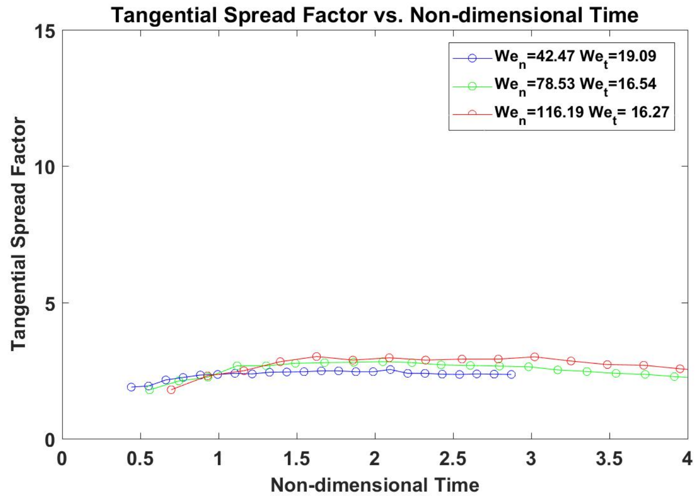


(a)

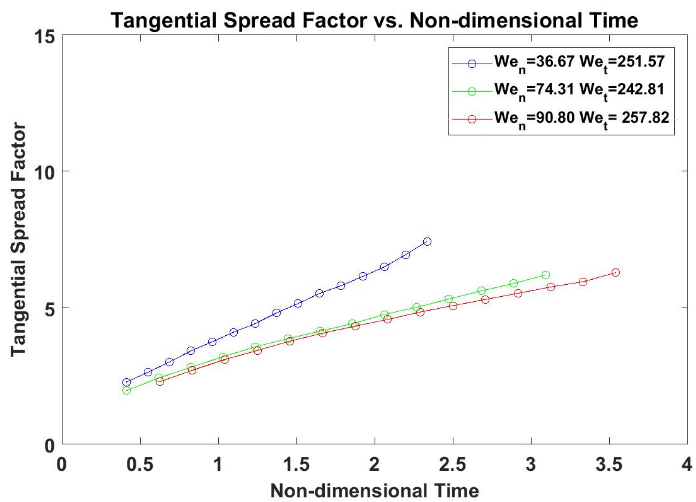


(b)

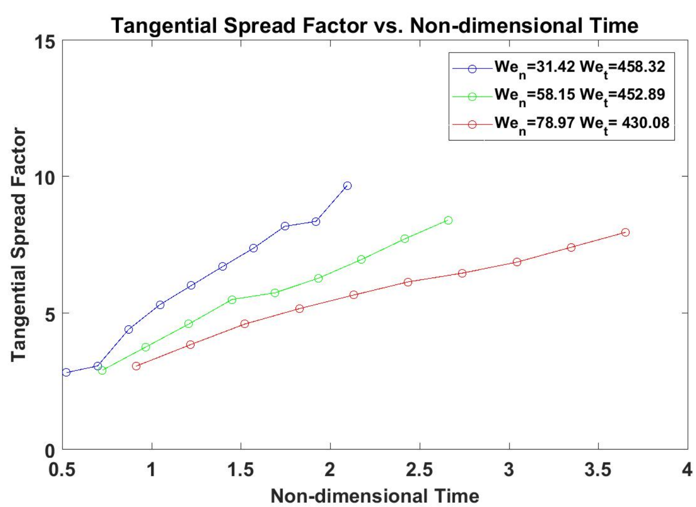


(c)

**Figure 34:** Effect of $We_n$ on tangential spread factor for hydrophobic surface

#### 5.1.1.3 *Effect of $We_n$ to Area Spread Factor at low, Moderate and High $We_t$*

Effect of $We_n$ onto area spread factor at low,moderate and high $We_t$ can be seen figure 35. Area spread factor rises as $We_n$ increases at low $We_t$. However, it is seen that after increase in $We_t$, area spread factor does not depend $We_n$ at moderate and high $We_t$. It seems that mostly effect of $We_t$ determines the spread area factor. It can be seen from the figure 25, there is transition area when $We_t$ is around 250. Therefore, there are inconsistent area spread factor data for the effect of $We_n$ at moderate $We_t$. This gives idea about the outcome changes in the regime map.

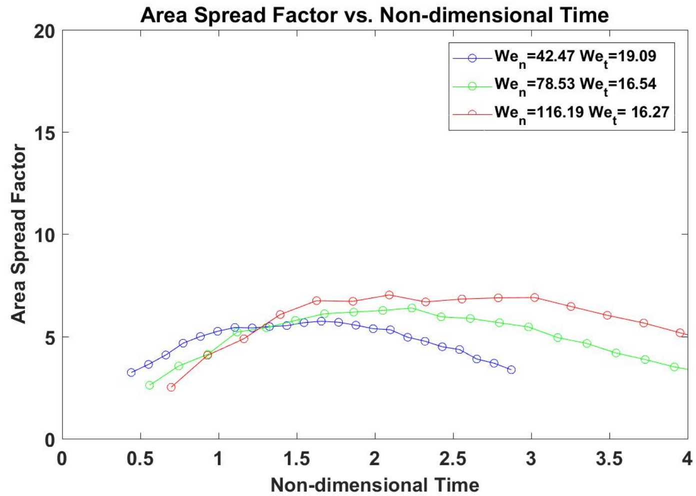


(a)

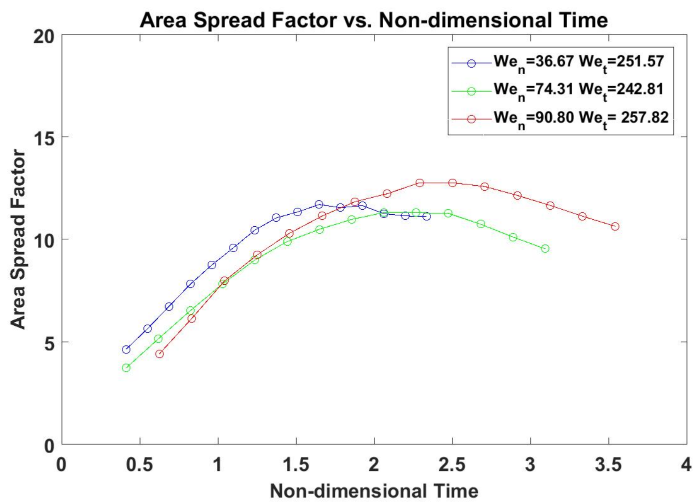


(b)

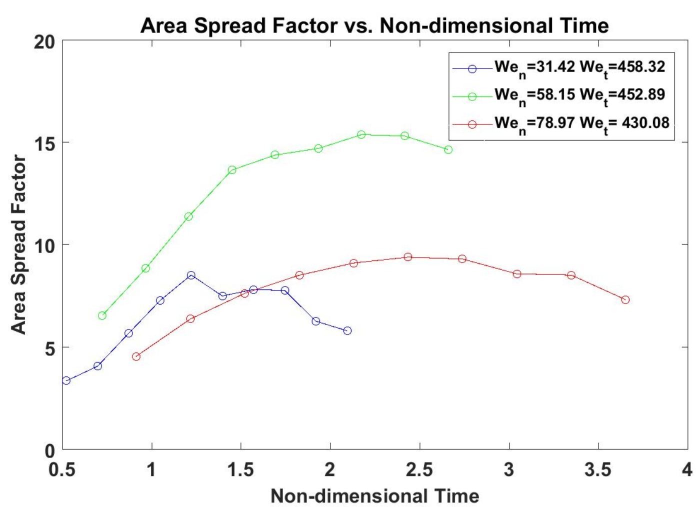


(c)

**Figure 35:** Effect of $We_n$ on area spread factor for hydrophobic surface

### 5.1.2 Effect of $We_t$ on Spreading for Hydrophobic Smooth Surface

#### *5.1.2.1 Effect of $We_t$ on Radial Spread Factor at low, Moderate and High $We_n$*

Effect of $We_t$ to radial spread factor at low, moderate and high $We_n$ can be seen at figure 36. $We_t$ does not have crucial affect on radial spreading at low and moderate $We_n$. But it is inversely proportional with radial spreading at high $We_n$ so at the higher $We_t$, the lower radial spreading on the surface.

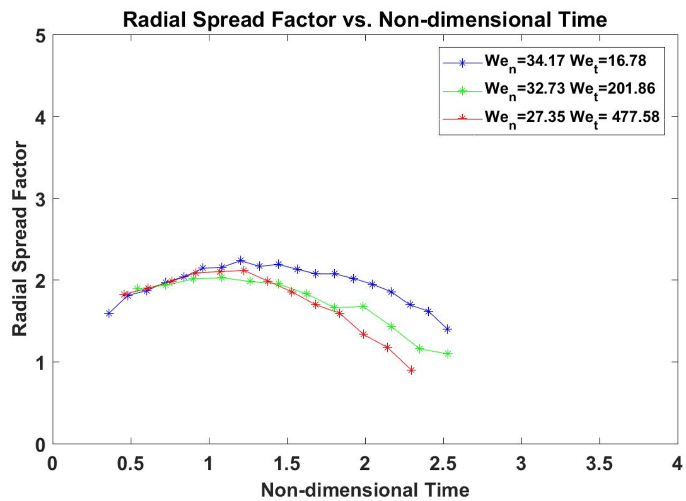


(a)

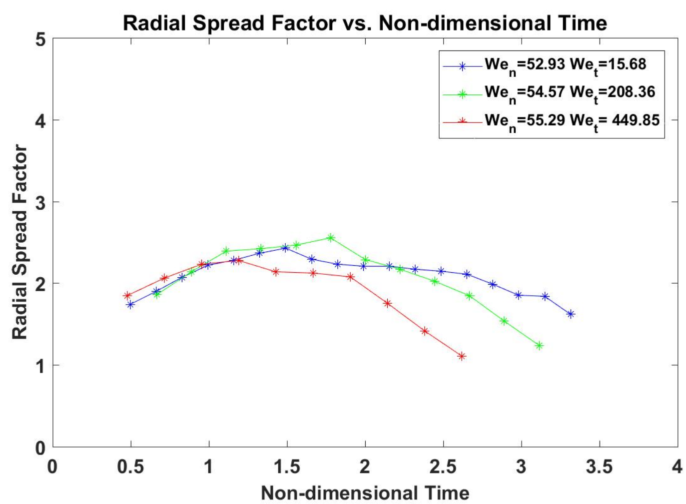


(b)

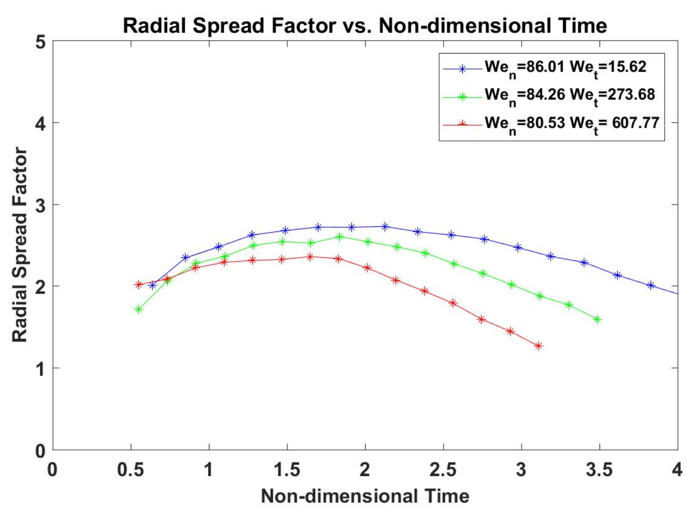


(c)

**Figure 36:** Effect of $We_t$ on radial spread factor for hydrophobic surface

#### 5.1.2.2 *Effect of $We_t$ on Tangential Spread Factor at low, Moderate and High $We_n$*

Influence of $We_t$ onto tangential spread factor is shown in figure 37. When $We_t$ increased, tangential spreading on the surface increases for all $We_n$. However, $We_n$ is a significant parameter for the maximum tangential spreading. If $We_n$ of the droplet increases, maximum tangential spreading on the surface decreases. It can be seen from the figure 37 when low $We_n$ case compared with moderate and high $We_n$ cases.

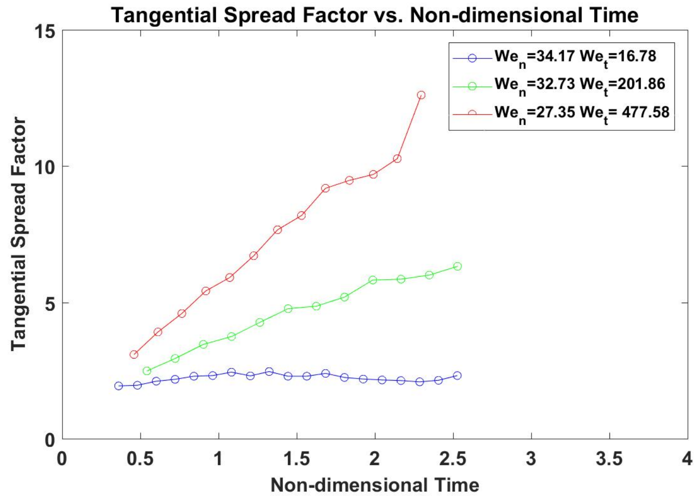


(a)

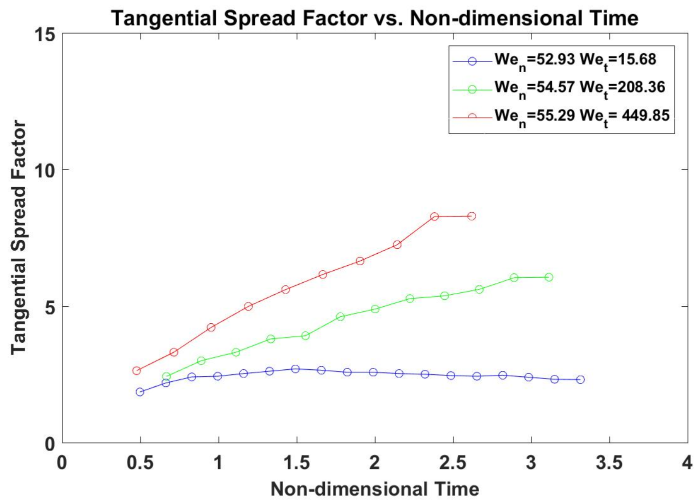


(b)

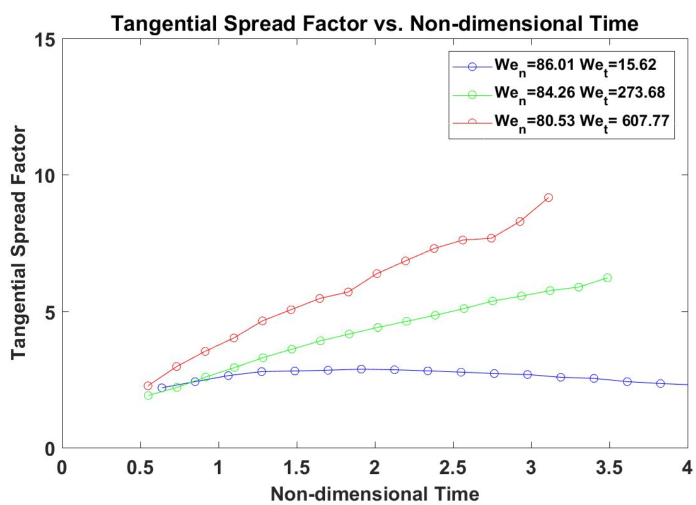


(c)

**Figure 37:** Effect of $We_t$ on tangential spread factor for hydrophobic surface

#### 5.1.2.3 *Effect of $We_t$ on Area Spread Factor at low, Moderate and High $We_n$*

The effect of $We_t$ to the area spread factor can be seen in figure 38. Area spread factor increases when $We_t$ increased for all cases. The maximum area spread factor is reached when $We_n$ and $We_t$ is high.

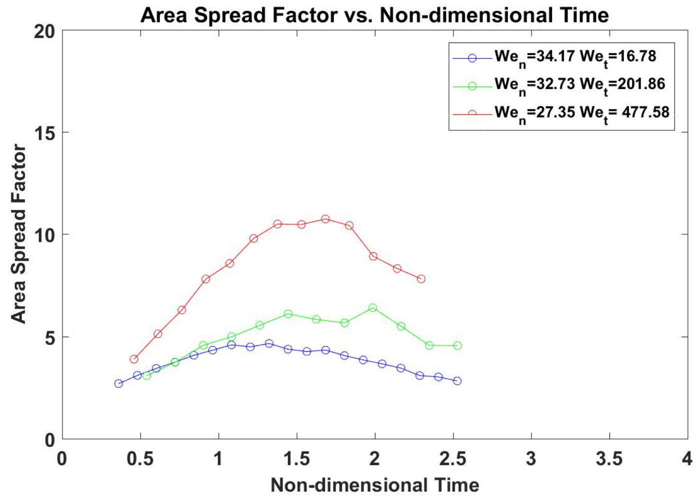


(a)

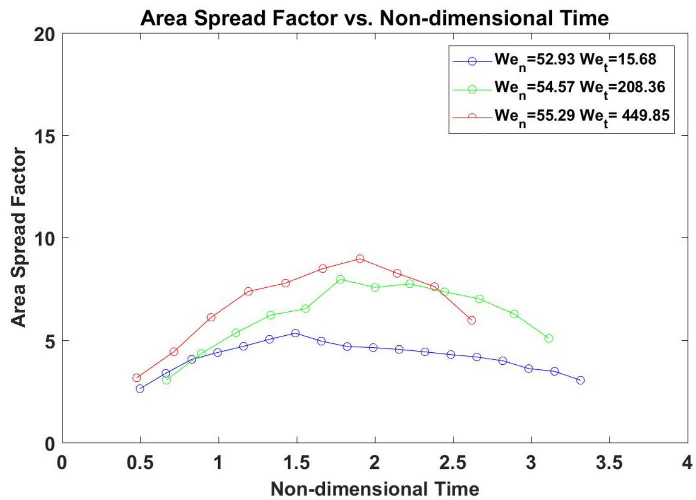


(b)

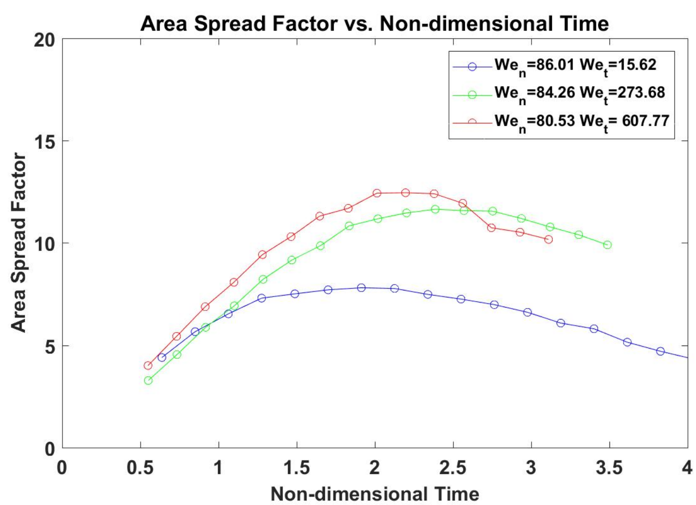


(c)

**Figure 38:** Effect of $We_t$ on area spread factor for hydrophobic surface

## 5.2 Drop Impact Spreading on Moving Hydrophilic Smooth Surface

On the hydrophilic surface, it hits and forms ellipse shape lamella. After it reached maximum spreading, it cannot recede much because of low receding contact angle but liquid sheet moves radially outwards at t=0.0009375s (Figure 32). Effect of $We_n$ and $We_t$ have been examined on radial, tangential and area spread factor. In the study, effect of $We_n$ and $We_t$ on spreading has been investigated on hydrophilic surface. First, effect $We_n$ is observed while $We_t$ kept constant at low, moderate and high. Then influence of $We_t$ is investigated while $We_n$ kept constant at low, moderate and high. Spreading analysis started just after droplet hits to surface and finished until any reflection or splitting is observed at the image. Therefore, droplet spreading cannot be presented as full cycle for the cases but advancing and some part of the receding phase of the spreading was measured for all cases.

### 5.2.1 Effect of $We_n$ on Spreading for Hydrophilic Smooth Surface

#### *5.2.1.1 Effect of $We_n$ on Radial Spread Factor at Low, Moderate and High $We_t$*

It can be seen from the figure 39 that, radial spreading increases on hydrophilic surface as $We_n$ rises for all cases. Because droplet hits to surface and expands more when $We_n$ is higher.

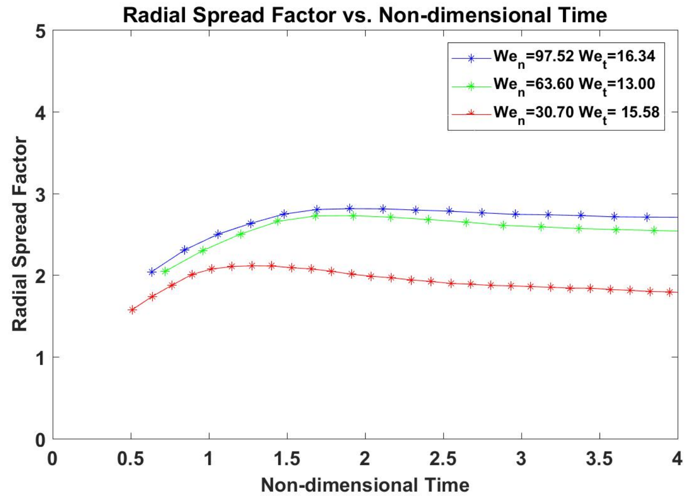


(a)

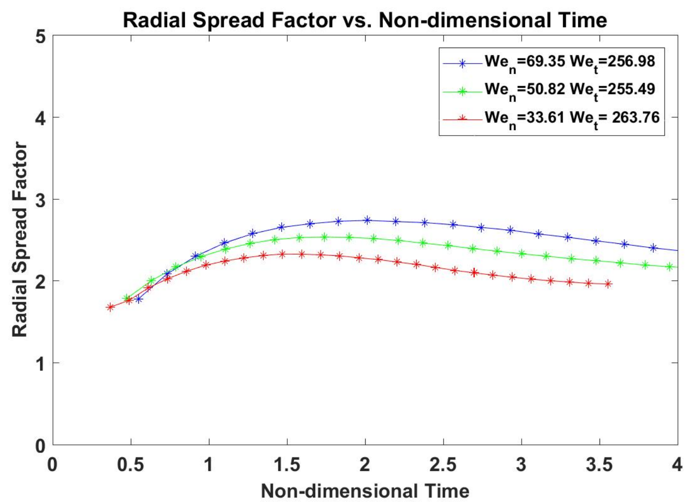


(b)

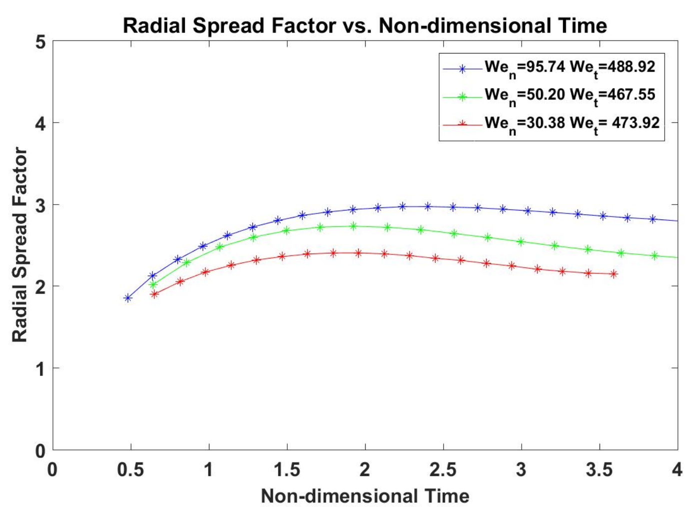


(c)

**Figure 39:** Effect of $We_n$ on radial spread factor for hydrophilic surface

#### *5.2.1.2 Effect of $We_n$ on Tangential Spread Factor at Low, Moderate and High $We_t$*

Tangential spreading rises as $We_n$ increases at low $We_t$ case. Since $We_t$ is low, lamella expands in all directions and this causes similar radial and tangential spreading. However, tangential spreading reduces when $We_n$ is increased at moderate and high $We_t$ (Figure 40).

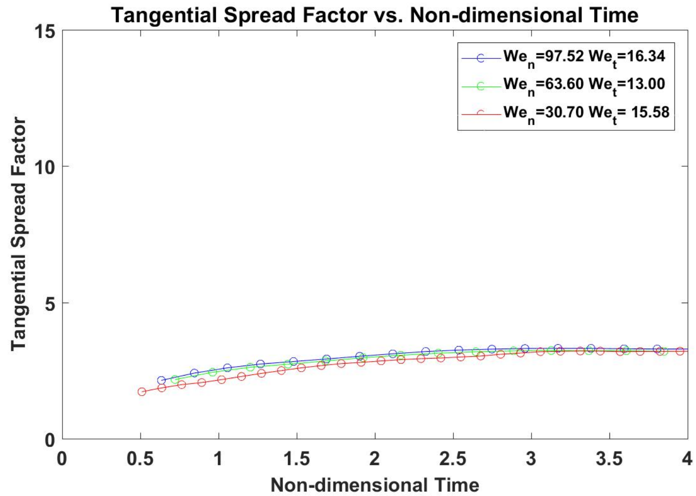


(a)

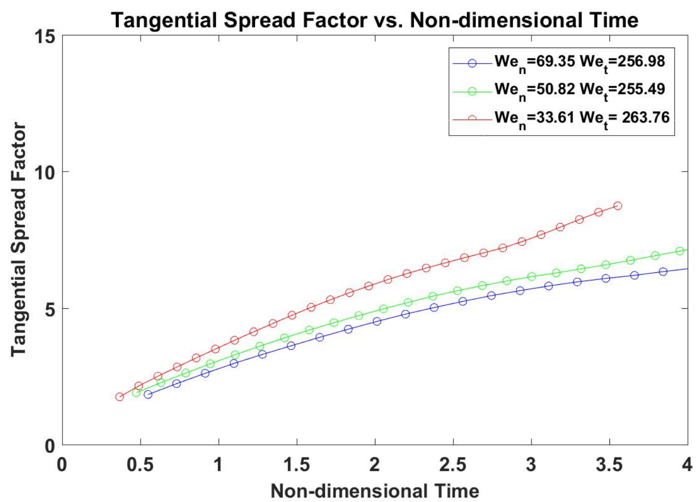


(b)

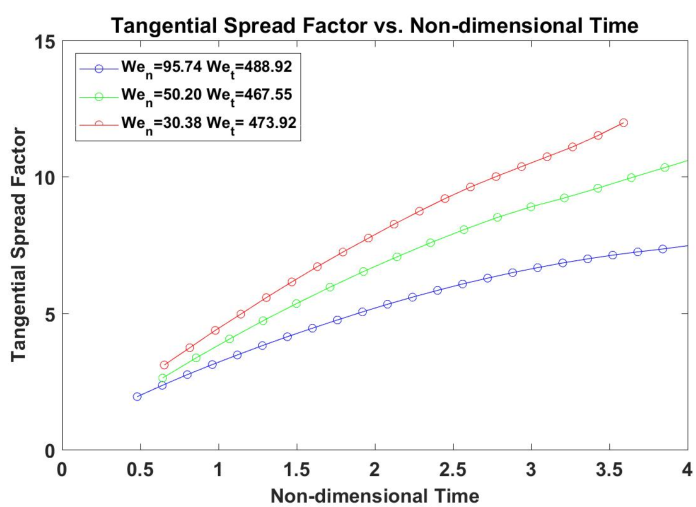


(c)

**Figure 40:** Effect of $We_n$ on tangential spread factor for hydrophilic surface

#### *5.2.1.3 Effect of $We_n$ on Area Spread Factor at Low, Moderate and High $We_t$*

Area spread factor rises as $We_n$ increased at low $We_t$. Since $We_t$ is low surface movement cannot influence lamella significantly. However, at moderate and high $We_t$, increase in the $We_n$ decreases the area spread factor. Moreover, maximum area spread factor is reached when $We_n$ is low and $We_t$ is high.

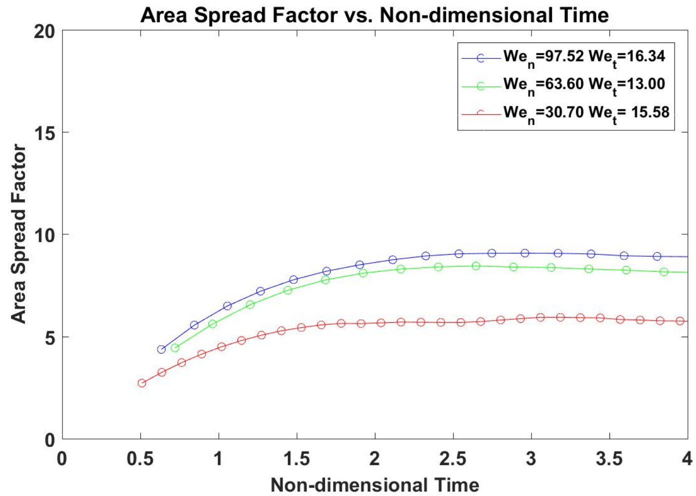


(a)

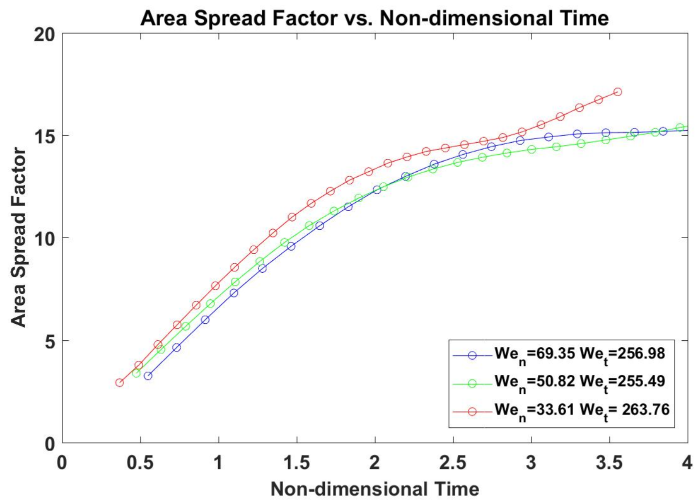


(b)

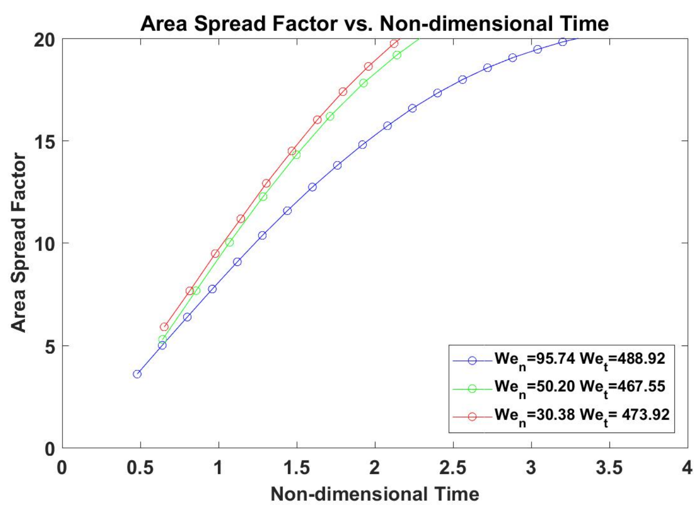


(c)

**Figure 41:** Effect of $We_n$ on area spread factor for hydrophilic surface

### 5.2.2 Effect of $We_t$ on Spreading for Hydrophilic Smooth Surface

#### 5.2.2.1 *Effect of $We_t$ on Radial Spread Factor at low, Moderate and High $We_n$*

$We_t$ does not have crucial affect on radial spreading at low, moderate and high $We_n$ at advancing phase (Figure 42). However, it affects lamella at the receding phase in low $We_n$ case. Lamella recedes if the $We_t$ and $We_n$ are low and when $We_t$ increases, radial spread factor at the receding phase decreases. Furthermore, maximum radial spreading is observed at the high $We_n$ case.

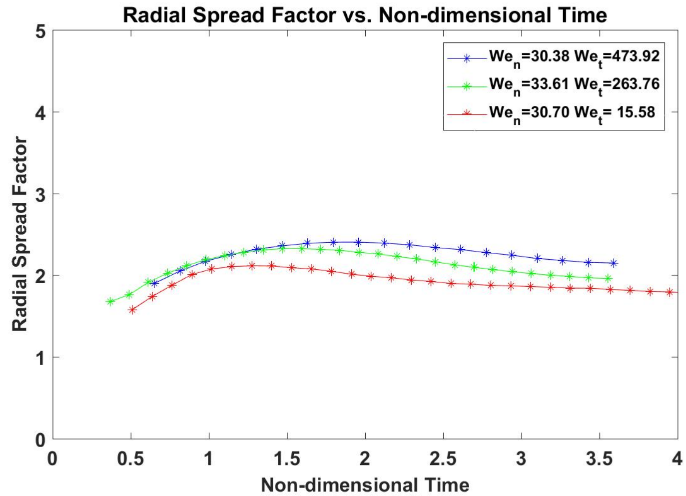


(a)

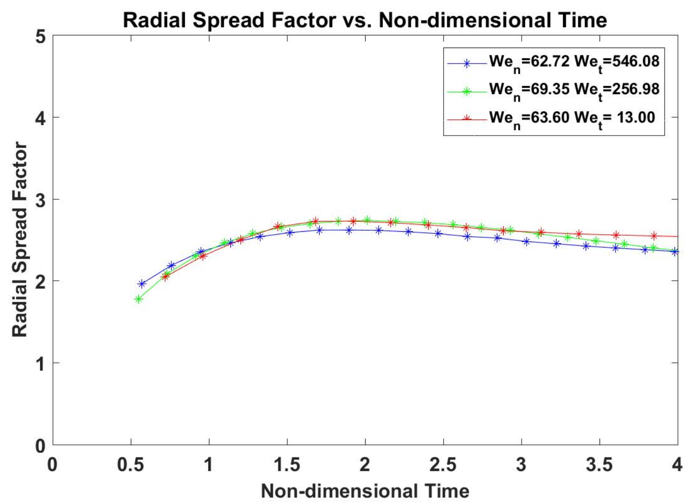


(b)

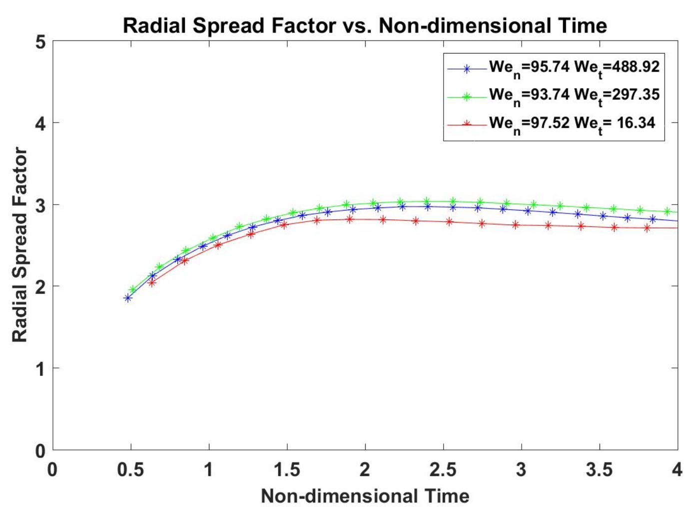


(c)

**Figure 42:** Effect of $We_t$ on radial spread factor for hydrophilic surface

#### 5.2.2.2 *Effect of $We_t$ on Tangential Spread Factor at low, Moderate and High $We_n$*

Effect of $We_t$ on tangential spread factor at different $We_n$ is shown in figure 43. It can be seen that, tangential spread factor increases as $We_t$ rises for all cases. According to the figures, lamella does not recede in the tangential direction so it elongates with the surface movement.

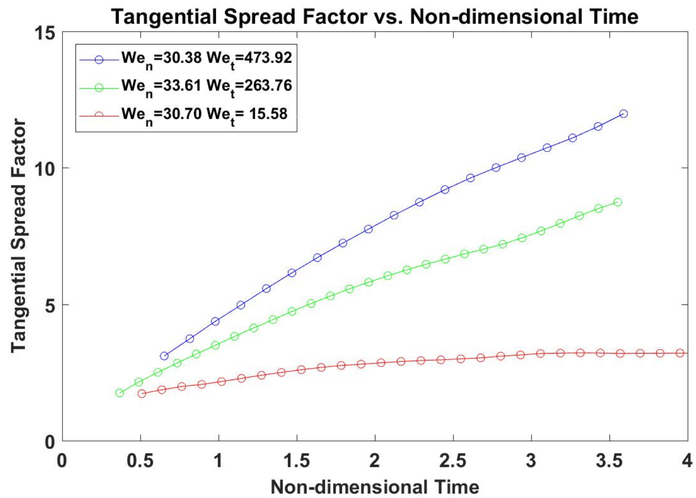


(a)

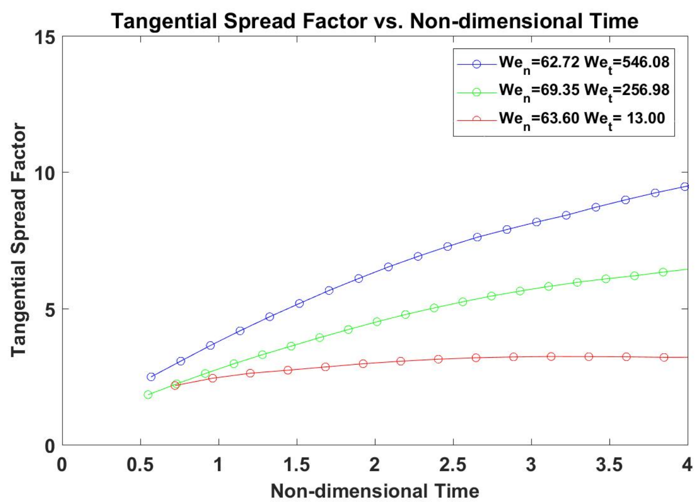


(b)

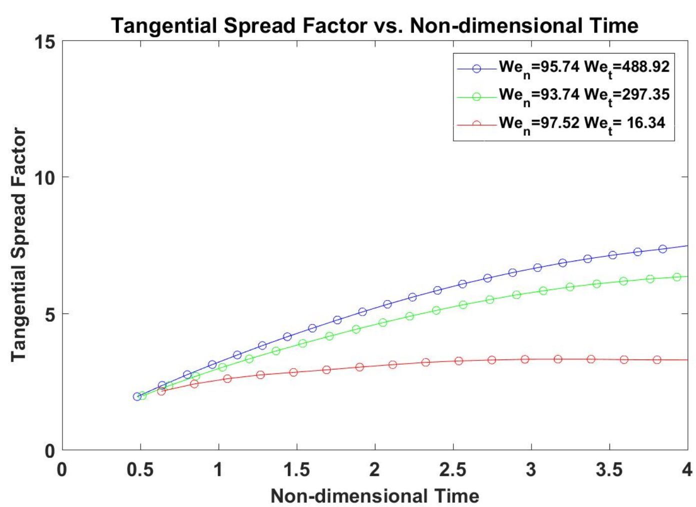


(c)

**Figure 43:** Effect of $We_t$ on tangential spread factor for hydrophilic surface

#### 5.2.2.3 *Effect of $We_t$ on Area Spread Factor at low, Moderate and High $We_n$*

Area spread factor rises when $We_t$ increased for all cases (Figure 44). Since the surface is hydrophilic, it holds the lamella and effect of the surface movement increases. Therefore, area spread factor of lamella on hydrophilic surface is determined by $We_t$ mostly at low and moderate $We_n$. Effect of $We_n$ started to be seen when it reached around 90 and it decreases maximum area spread factor at $We_t$= 488.92. Therefore, maximum area spread factor can be reached when $We_n$ is low and $We_t$ is high.

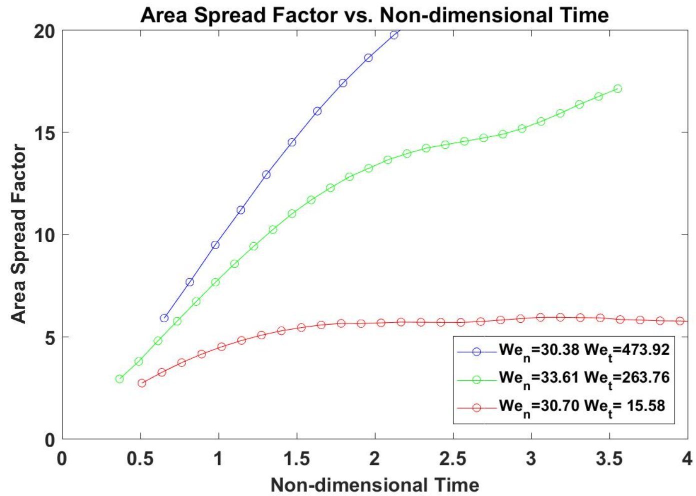


(a)

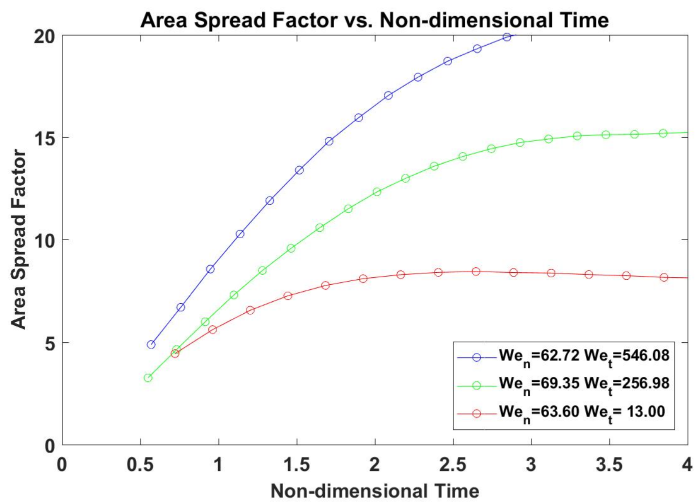


(b)

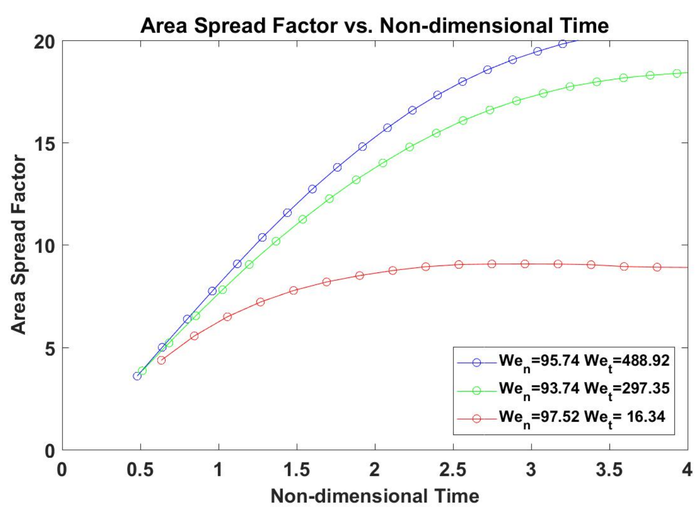


(c)

**Figure 44:** Effect of $We_t$ on area spread factor for hydrophilic surface

# CHAPTER VI

# DISCUSSION

The regime map of present study looks similar with the study which has done by Chen and Wang[6] where Teflon has been used as smooth hydrophobic moving surface. There are differences in the regime maps, most probably because of the difference in the dynamic contact angles. Static contact angle of their study is 103° which is close to our case. However, advancing and receding angle of Teflon reported as 142° and 82°, respectively. In other words, Teflon surface has higher advancing and receding contact angle than those of paraffin used in the present study. In addition to observed behaviors by Chen and Wang[6], deposition with trailing edge split was observed in the present study, because of the higher $We_t$ range and the lower dynamic contact angle values.

When advancing and receding contact angle of the surface decreased, droplet is exposed to the surface for a longer time and, therefore, effect of the moving surface increases and alteration in regime maps occurs. Since the effect of moving surface is increased, split deposition and deposition with trailing edge split are seen at lower $We_t$ values. Moreover,in the present study, deposition with vertical split cannot be seen except when $We_t$=0. Because of the low receding and advancing contact angle, droplet is stretched more in the direction of surface motion than those impacting to the Teflon surface. Furthermore, energy dissipation increases in the droplet and consequently, droplet cannot create upward jet and deposits on the surface at low $We_t$ values, at which deposition with vertical split was observed on the Teflon surface.

Almohammadi and Amirfazli[5] has recently studied droplet impact on moving hydrophilic and hydrophobic smooth surfaces in a larger range of $We_t$ and $We_n$ but with a coarser resolution than those of present study. Receding and advancing contact angles are reported as $89 \pm 1°$ and $34 \pm 2°$ for hydrophilic smooth case and $123 \pm 1°$ and $109 \pm 1°$ for hydrophobic smooth case, respectively. Regime maps in this study do not look similar with the present ones because of higher advancing and receding contact angles of their hydrophobic and hydrophilic surfaces. For the hydrophobic case, rebound and stretch rebound has been reported by Almohammadi and Amirfazli[5] over $We_t < 900$ and $We_n < 180$ range, where we observed deposition with vertical split, deposition, split deposition and deposition with trailing edge split. This difference is due to the lower contact angles in the present investigation. Nevertheless, rebound and stretch rebound have been also observed in the present study for the superhydrophobic surfaces (Figures 18-20), but they are classified as the rebound outcome. For the hydrophilic case, Almohammadi and Amirfazli[5] have observed deposition and recoiling over $We_t < 900$ and $We_n < 160$ range, where deposition, deposition with trailing edge droplet formation and deposition with trailing edge split have been observed in the present study (Figure 29). Recoiling is observed as a part of the last two behavior (Figures 27-28). Due to low receding and advancing angles of the hydrophilic surface in the present study, droplets could be stretched more and, consequently, at the trailing edge the droplet formation and splitting could be observed.

While visualizing droplet impact, effect of centrifugal force was observed only with the hydrophilic surfaces. Because of low advancing and receding contact angles, lamella advancing and receding phase take more time on the surface and rotational surface motion starts to influence the outcome. Views of drop impact at $t = 0.001375\,s$ on the smooth hydrophilic, hydrophobic and superhydrophobic surfaces can be seen in the figure 45. On the hydrophilic surface, drop impact is at the receding phase and lamella starts to flow radially outward due to centrifugal force, whereas, receding is completed on the hydrophobic and superhydrophobic surfaces. This effect on the lamella starts for $We_t > 50$ for hydrophilic surfaces. An important question to be answered is how far the centrifugal forces effects the observed outcomes and the regime maps. Droplet impact outcome development on smooth hydrophilic surface can be seen in figure 46. It shows that receding starts earlier at the trailing edge and both side of the rim impacts. Then, because of the surface movement accumulated part creates splitting at the trailing edge.


(a)


(b)


(c)

**Figure 45:** Effect of rotation , (a) hydrophilic smooth surface - Deposition with trailing edge split ($We_n$= 31.54 $We_n$=549.76), (b) Hydrophobic Smooth Surface - Deposition with trailing edge split ($We_n$= 29.47 $We_n$= 540.09), (c) Superhydrophobic Smooth Surface - Rebound ($We_n$= 27.64 $We_n$= 545.07)

Effect of roughness was studied on splashing by Mundo et.al.[4]. They created a nondimensional parameter which is $S_t$ to define surface roughness. It is the ratio of peak to valley distance over the entire measured array and initial droplet diameter. When $S_t$ values compared, the roughness levels of the present study classified as smooth. However, we observed that those small roughness values affect splashing and droplet impact outcome. Splashing is not seen at the superhydrophobic smooth case. It is observed at the superhydrophobic moderate rough and rough cases and their $St$ values are 0.07 and 0.09, respectively. On the other hand, splashing cannot be observed at the hydrophobic and hydrophilic rough cases (Figures 26 - 30). Although, superhydrophobic moderate and hydrophilic rough case have same $S_t$ values, splashing cannot be seen at the hydrophilic one. Therefore, it seems that splashing not only depends on the roughness but also wettability of the surface. In addition to splashing, it may cause outcome change or earlier splitting. While deposition with vertical split is observed at the hydrophobic smooth surface at $We_t = 0$, it cannot be seen at the rough (Figures 25 - 26). It also leads to much earlier splitting on the hydrophilic rough case. Deposition with trailing edge split observed when $We_t > 300$ on the smooth case whereas it reduced to $We_t > 75$ on the rough one (Figures 29 - 30 ).

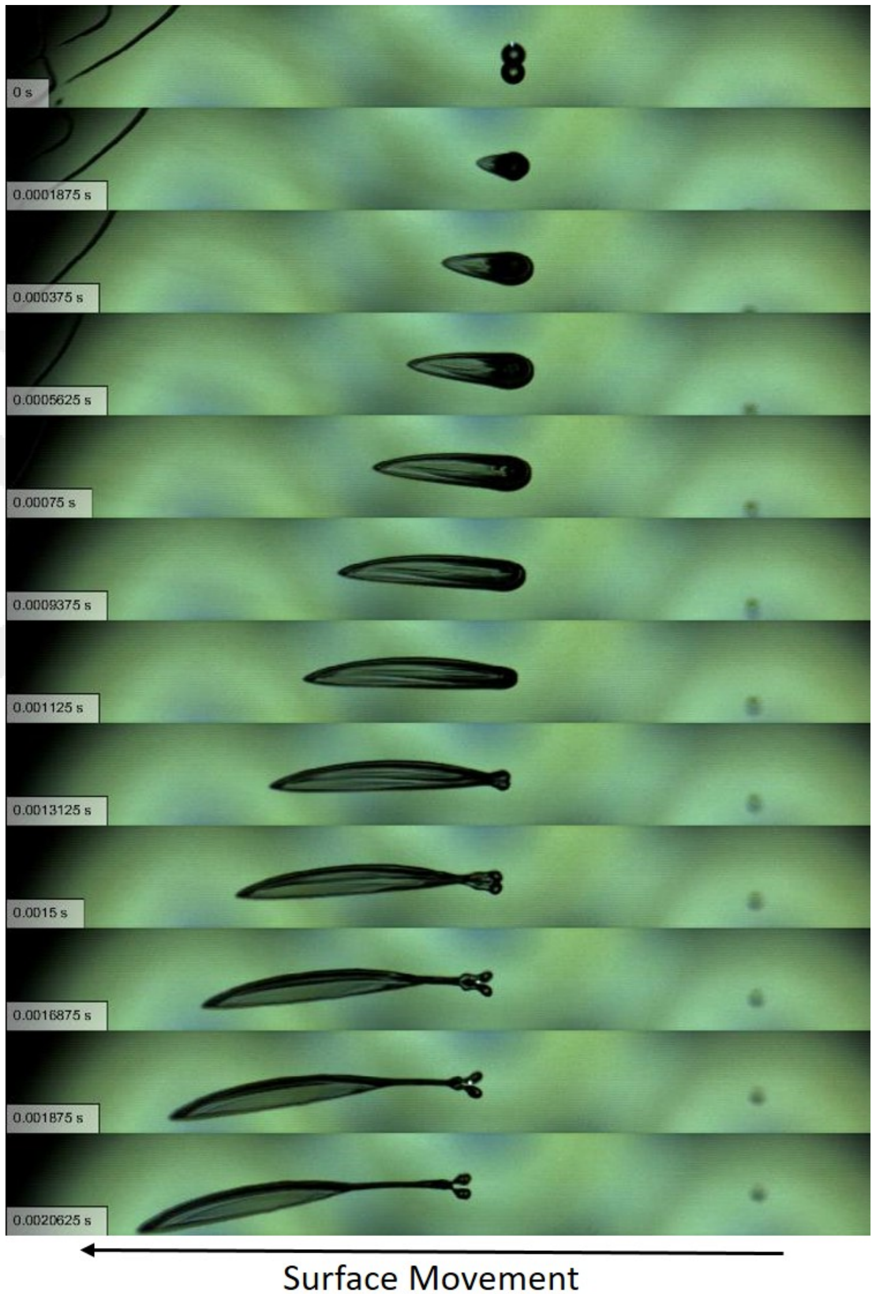


**Figure 46:** Droplet impact development on hydrophilic smooth surface - Deposition with trailing edge split ($We_n$= 31.54 $We_n$=549.76)

# CHAPTER VII

# CONCLUSION

Droplet behavior on moving surfaces have been studied by changing $We_n$ , $We_t$ , contact angle and surfaces roughness. Experiments have been done for three different surface types (superhydrophobic, hydrophobic and hydrophilic) and different levels of roughness (smooth, moderate rough and rough). Regime maps were constructed by using normal and tangential Weber numbers and it is observed that dynamic contact angle and roughness of the surface is significant parameters for the droplet behavior. Observed droplet outcomes on superhydrophobic, hydrophobic and hydrophilic surfaces depending on $We_n$, $We_t$ and effect of the roughness to droplet behavior summarized as below:

**Superhydrophobic Surface**

- At the low $We_t$ and $We_n$, rebound and rebound with vertical split can be observed depending on the surface roughness. Rebound with vertical split is seen at smooth case and rebound is observed at moderate rough and rough cases.

- When $We_n$ increased at the low $We_t$, receding breakup with rebound is seen at moderate rough and rough cases. Splashing is observed in both of the cases but it is seen earlier at rough case.

- At the high $We_t$, splitting from the leading edge with rebound is seen.

- Rebound with both sides split is the outcome of droplet impact at the high $We_n$ and $We_t$.

**Hydrophobic Surface**

- Deposition with vertical split is seen when $We_t$=0 on smooth hydrophobic surface. However, it cannot be observed at the rough case due to roughness effect.
- Deposition is observed at low $We_t$ on smooth and rough cases.
- When $We_t$ increases, behavior turns into split deposition.
- Even more increase in $We_t$ causes splitting at the trailing edge of the droplet (deposition with trailing edge split).

**Hydrophilic Surface**

- At the low $We_t$, droplet deposits on the surface.
- If the $We_t$ increases more, it elongates on the surface with the droplet formation at the trailing edge.
- When $We_t$ increases much more, deposition with trailing edge split is seen.
- In the hydrophilic case roughness plays a significant role in the trailing edge split. If the surface is rough, drops are splitted from the trailing edge at earlier $We_t$ than smooth one.

**Effect of Roughness**

- High roughness values of the surface may trigger splashing depending on normal Weber number of the droplet.
- In addition to splashing, it reduces $We_t$ threshold for the horizontal splitting depending on the surface types.

Furthermore, droplet spreading on moving hydrophilic and hydrophobic surfaces have been investigated by changing $We_n$ and $We_t$. Radial, tangential and area spread factor have been plotted with respect to nondimensional time for the surfaces.

The influence of $We_n$ and $We_t$ to radial, tangential and area spread factor on hydrophobic surface stated as:

- Radial spread factor rises as $We_n$ increases on the hydrophobic surface. Maximum spreading at radial direction is reached when $We_t$ is low and $We_n$ is high.

- Tangential spread factor increases as $We_n$ increases at low $We_t$. Also, it rises when $We_n$ reduces and $We_t$ increases. Maximum tangential spreading is reached when $We_n$ is low and $We_t$ is high.

- Area spread factor rises as $We_n$ increases at low $We_t$. When $We_t$ rises, area spread factor increases at for all $We_n$ cases.

Also, change in $We_n$ and $We_t$ affects radial, tangential area spread factor on hydrophilic surface as followed:

- Rise in $We_n$ increases radial spread factor on hydrophilic surfaces. However, it seems that $We_t$ does not have crucial influence to radial spreading on hydrophilic surface. Maximum radial spreading is observed at high $We_n$.

- Tangential spread factor increases as $We_n$ increases at low $We_t$. It rises as $We_t$ increases and maximum tangential spread factor is reached when $We_n$ is low and $We_t$ is high.

- Area spread factor rises as $We_n$ increases at low $We_t$. If $We_n$ rises, area spread factor reduces at moderate and high $We_t$. When $We_t$ rises, area spread factor increases and lamella reaches maximum area spread factor at low $We_n$ and high $We_t$ on hydrophilic surface.

## 7.1 Future Work

Droplet spreading on rough hydrophilic, rough hydrophobic and superhydrophobic cases cannot be completed because of image processing problems. They will be measured and reported to demonstrate the effect of high contact angle and roughness to droplet lamella development. Furthermore, droplet impact onto vibrating surface is going to be studied by changing $We_n$, contact angle and vibration frequency. Study aims to find out a new atomization method by vibrating the surface at high frequency.

# Bibliography


[1] R. Rioboo, C. Tropea, and M. Marengo, "Outcomes from a drop impact on solid surfaces," *At. Sprays*, vol. 11, no. 2, pp. 155–165, 2001.

[2] R. Rioboo, M. Marengo, and C. Tropea, "Time evolution of liquid drop impact onto solid , dry surfaces," *Exp. Fluids*, vol. 33, pp. 112–124, jul 2002.

[3] A. Yarin, a.L. Yarin, and A. Yarin, "DROP IMPACT DYNAMICS: Splashing, Spreading, Receding, Bouncing…," *Annual Review of Fluid Mechanics*, vol. 38, pp. 159–192, jan 2006.

[4] C. Mundo, M. Sommerfeld, and C. Tropea, "Droplet-wall collisions: Experimental studies of the deformation and breakup process," *Int. J. Multiph. Flow*, vol. 21, no. 2, pp. 151–173, 1995.

[5] H. Almohammadi and A. Amirfazli, "Understanding the drop impact on moving hydrophilic and hydrophobic surfaces," *Soft Matter*, vol. 13, no. 10, pp. 2040–2053, 2017.

[6] R. H. Chen and H. W. Wang, "Effects of tangential speed on low-normal-speed liquid drop impact on a non-wettable solid surface," *Experiments in Fluids*, vol. 39, no. 4, pp. 754–760, 2005.

[7] J. C. Bird, S. S. H. Tsai, and H. a. Stone, "Inclined to splash: triggering and inhibiting a splash with tangential velocity," *New J. Phys.*, vol. 11, p. 63017, jun 2009.

[8] J.-Y. Li, X.-F. Yuan, Q. Han, and G. Xi, "Impact patterns and temporal evolutions of water drops impinging on a rotating disc," *Proceedings of the Institution*

*of Mechanical Engineers, Part C: Journal of Mechanical Engineering Science*, vol. 226, no. 4, pp. 956–967, 2012.

# APPENDIX A

# SOME ANCILLARY STUFF

## A.1 Droplet Recognition and Calculation of Nondimensional Numbers

```
close all
clear all
clc
%% Fluid Properties- WATER
rho= 998.2;  %kg/m3I_1
mu=1.002*10^-3;
sigma= 0.072; %N/m
fps=16000;
R= 0.0225; %m
%%
failedFiles = {};
%Reference Image Processing
reference_length = 0.001; %m % 44 pixel = 1 mm is reference length
t=1/fps ; %sec
img = imread('calibration(1mm).bmp');
bw = im2bw(img);
bw_1=imcrop(bw);
%%
imshow(bw_1)
```

```
Rmin=15;
Rmax=40;
[centersDark, radiiDark] = imfindcircles(bw_1,[Rmin Rmax],'ObjectPolarity','dark','EdgeThreshold', 0.2) ; %Finds first droplet ----------------------
viscircles(centersDark, radiiDark,'LineStyle','--', 'EdgeColor', 'b');
h = imdistline(gca, [centersDark(1)-radiiDark centersDark(1)+radiiDark] ,[centersDark(2) centersDark(2)]);
api = iptgetapi(h);
fcn = makeConstrainToRectFcn('imline',...
    get(gca,'XLim'),get(gca,'YLim'));
api.setDragConstraintFcn(fcn);
unit_length_pix = 2*radiiDark;

%%
%Take Out The Desired Frames
Files=dir('C:\Users\user\Google Drive\TUBITAK 1001\Fluid Mechanics\Droplet Videos_ALL\Droplet Videos with Selenoid\With New Lens\Distilled Water\Slanted Videos_16000_fps\SH_Smooth\*.mp4');
N=5;  % No of Frames
for i=1:length(Files)
    figure
    a0=(Files(i));
    Finddash= strfind(a0.name, '_');
    Findr=strfind(a0.name,'r');
```

```
RPM(i,1)= str2double (a0.name(Finddash(1)+1:Findr(1)-1));
Name=a0.name;% Take out the motor RPM to calculate
    tangential We number
[behavior,behavior_num]=BehaviorName(Finddash,Name);
behaviornumber(i,:)= str2num(behavior_num);
a=VideoReader (a0.name);
[z,rect]=imcrop(read (a,1));
for img = 1:N;
    bc= read (a,img);
    b{img}=imcrop(bc,rect);
end
%% Make all the frames gray-scale
for k = 1:N
    I_1{k}= rgb2gray(b{k});
    I_adjust{k}= imadjust(I_1{k});
  end
% Merge Frames and find the different diameters
for j=1:N-1
    image1=I_adjust{j};
    image2=I_adjust{j+1};
    C = imfuse(image1,image2,'blend','Scaling','joint');
        %---------------
    imshow(C);
    Rmin=8;
    Rmax=15;
```

```
[centersDark, radiiDark] = imfindcircles(image1,[Rmin Rmax],'ObjectPolarity','dark','EdgeThreshold', 0.3);  %Finds first droplet ---------------------
[centersDark1, radiiDark1] = imfindcircles(image2,[Rmin Rmax],'ObjectPolarity','dark','EdgeThreshold', 0.3); %Finds second droplet
if isempty(centersDark)||isempty(centersDark1)
    Rmin=15;
    Rmax=40;
    [centersDark, radiiDark] = imfindcircles(image1,[Rmin Rmax],'ObjectPolarity','dark','EdgeThreshold', 0.3);  %Finds first droplet ---------------------
    [centersDark1, radiiDark1] = imfindcircles(image2,[Rmin Rmax],'ObjectPolarity','dark','EdgeThreshold', 0.3); %Finds second droplet
    if isempty(centersDark) ||isempty(centersDark1)
        Rmin=45;
        Rmax=110;
        [centersDark, radiiDark] = imfindcircles(image1,[Rmin Rmax],'ObjectPolarity','dark','EdgeThreshold', 0.3);  %Finds first droplet ---------------------
        [centersDark1, radiiDark1] = imfindcircles(image2,[Rmin Rmax],'ObjectPolarity','dark','EdgeThreshold', 0.3); %Finds second droplet
```

```
            end
        end
        if isempty(centersDark)||isempty(centersDark1) ;
            failedFiles {i} = filename ;
            continue
        end
        viscircles(centersDark, radiiDark,'LineStyle','--', 'EdgeColor', 'b');
        h = imdistline(gca, [centersDark(1)-radiiDark centersDark(1)+radiiDark] ,[centersDark(2) centersDark(2)]);
        api = iptgetapi(h);
        fcn = makeConstrainToRectFcn('imline',...
            get(gca,'XLim'),get(gca,'YLim'));
        api.setDragConstraintFcn(fcn);
        viscircles(centersDark1, radiiDark1,'LineStyle','--', 'EdgeColor', 'b');
        h2 = imdistline(gca, [centersDark(1) centersDark(1)] ,[centersDark(2)-radiiDark centersDark1(2)-radiiDark]);
        api = iptgetapi(h2);
        fcn = makeConstrainToRectFcn('imline',...
            get(gca,'XLim'),get(gca,'YLim'));
        api.setDragConstraintFcn(fcn);
        Displacement(j)= centersDark1(1,2)- centersDark(1,2); %in pixels
    end
```

```
    %Calculate diameter and velocity
    Disp= sum(Displacement)/ (N-1);
    x= (Disp*reference_length)/unit_length_pix; %in m
    if isempty(centersDark)||isempty(centersDark1) ;
        continue
    else
        D (i,:) = (2*radiiDark*reference_length)/
            unit_length_pix ;%in m
    end
    v (i,:)=x/t ;%m/s
    v_t (i,:)= ((2*3.14*RPM (i))/60)*R; %m/s
    We_n (i,:) = (rho* (v(i)^2) * D(i)) / sigma;
    We_t (i,:)= (rho* (v_t(i)^2) * D(i)) / sigma;
    Re(i,:)= (rho* v(i)* D(i)/ mu);
    Ro(i,:)= v(i)/ (v_t (i));
    Fc_F= (((2*3.14*RPM (i))/60)^2* R * D(i))/ (v(i)^2);
    Result{i,:}={a0.name D(i) v(i) Re(i) We_n(i) We_t(i) Ro(i
        ) behavior behaviornumber(i) Fc_F};
    format= 'Iteration %4.1f completed. \n';
    fprintf(format,i)
end
%Data in Table
for p=1:length(Files)
    if isempty(Result {p})
        result_table{p,1}={};
    else
        result_table(p,1:10)=Result{p};
```

```
        end
end
T=table(D,v,We_t,We_n,Re,'RowNames', {Files.name})
sprintf('- IMAGE PROCESSING COMPLETED - ')
```

### A.2 Droplet Spreading Image Processing Code

```
clc
clear all
close all
f=16000; %fps
Time=0;
rho= 998.2;  %kg/m3I_1
mu=1.002*(10^(-3));
sigma= 0.072; %N/m
fps=16000;
R= 0.0225; %m
t_cam=1/fps;
%% Image Calibration-Side View
reference_length = 0.001; %m
img = imread('1mm calibration.png');
bw = imadjust(rgb2gray(img),[0.2 0.5],[]);
bw_cropped=imcrop(bw);
imshow(bw_cropped)
Rmin=15;
Rmax=40;
```

```
[centersDark, radiiDark] = imfindcircles(bw_cropped,[Rmin Rmax],'ObjectPolarity','dark','EdgeThreshold', 0.2) ; % Finds first droplet --------------------
viscircles(centersDark, radiiDark,'LineStyle','--', 'EdgeColor', 'b');
h = imdistline(gca, [centersDark(1)-radiiDark centersDark(1)+radiiDark] ,[centersDark(2) centersDark(2)]);
api = iptgetapi(h);
fcn = makeConstrainToRectFcn('imline',...
     get(gca,'XLim'),get(gca,'YLim'));
api.setDragConstraintFcn(fcn);
unit_length_pix = 2*radiiDark;
%% Take Out The Desired Frames
Side_Files=dir('Z:\TUBITAK 1001\Fluid Mechanics\Spreading Experiments\Smooth Glass\Article Data\Smooth\High Wen-Low Wet\26cm_500rpm_7_1_tilted\Spreading\Processed\New folder\*.mp4');
N=5;  % No of Frames
for i=1:length(Side_Files)
     figure
     a0=(Side_Files(i));
     Finddash= strfind(a0.name, '_');
     Findr=strfind(a0.name,'r');
     RPM(i,1)= str2double (a0.name(Finddash(1)+1:Findr(1)-1));
     Name=a0.name;% Take out the motor RPM to calculate tangential We number
     [behavior,behavior_num]=BehaviorName(Finddash,Name);
```

```
behaviornumber(i,:)= str2num(behavior_num);
a=VideoReader (a0.name);
[z,rect]=imcrop(read (a,1));
 for img = 1:N;
    %filename= strcat (a0.name,'_',num2str (img), '.png');
    bc= read (a,img);
    b{img}=imcrop(bc,rect);
end
%% Make all the frames gray-scale
for k = 1:N
    I_1{k}= rgb2gray(b{k});
    I_adjust{k}= imadjust(I_1{k});
end
% Merge Frames and find the different diameters
for j=1:N-1
    image1=I_adjust{j};
    image2=I_adjust{j+1};
    C = imfuse(image1,image2,'blend','Scaling','joint'); %------------
    imshow(C);
    Rmin=7;
    Rmax=15;
    [centersDark, radiiDark] = imfindcircles(image1,[Rmin Rmax],'ObjectPolarity','dark','EdgeThreshold',0.2); %Finds first droplet ------------------
```

```
[centersDark1, radiiDark1] = imfindcircles(image2,[Rmin Rmax],'ObjectPolarity','dark','EdgeThreshold', 0.2); %Finds second droplet
if isempty(centersDark)||isempty(centersDark1)
    Rmin=15;
    Rmax=40;
    [centersDark, radiiDark] = imfindcircles(image1,[Rmin Rmax],'ObjectPolarity','dark','EdgeThreshold', 0.2);  %Finds first droplet
    [centersDark1, radiiDark1] = imfindcircles(image2,[Rmin Rmax],'ObjectPolarity','dark','EdgeThreshold', 0.2); %Finds second droplet
    if isempty(centersDark) ||isempty(centersDark1)
        Rmin=40;
        Rmax=75;
        [centersDark, radiiDark] = imfindcircles(image1,[Rmin Rmax],'ObjectPolarity','dark','EdgeThreshold', 0.2);  %Finds first droplet
        [centersDark1, radiiDark1] = imfindcircles(image2,[Rmin Rmax],'ObjectPolarity','dark','EdgeThreshold', 0.2); %Finds second droplet
    end
end
```

```
            viscircles(centersDark, radiiDark,'LineStyle','--', 'EdgeColor', 'b');
            h = imdistline(gca, [centersDark(1)-radiiDark centersDark(1)+radiiDark] ,[centersDark(2) centersDark(2)]);
            api = iptgetapi(h);
            fcn = makeConstrainToRectFcn('imline',...
                get(gca,'XLim'),get(gca,'YLim'));
            api.setDragConstraintFcn(fcn);
            viscircles(centersDark1, radiiDark1,'LineStyle','--', 'EdgeColor', 'b');
            h2 = imdistline(gca, [centersDark(1) centersDark(1)] ,[centersDark(2)-radiiDark centersDark1(2)-radiiDark]);
            api = iptgetapi(h2);
            fcn = makeConstrainToRectFcn('imline',...
                get(gca,'XLim'),get(gca,'YLim'));
            api.setDragConstraintFcn(fcn);
            Displacement(j)= centersDark1(1,2)- centersDark(1,2); %in pixels
    end
            %Calculate diameter and velocity
        Disp= sum(Displacement)/ (N-1);
        x= (Disp*reference_length)/unit_length_pix; %in m
        D_initial (i,:) = (2*radiiDark*reference_length)/unit_length_pix ;%in m
        v_initial (i,:)=x/t_cam ;%m/s
```

```
        v_t (i,:)= ((2*3.14*RPM (i))/60)*R; %m/s
        We_n (i,:) = (rho* (v_initial(i)^2) * D_initial(i)) /
            sigma;
        We_t (i,:)= (rho* (v_t(i)^2) * D_initial(i)) / sigma;
        Re(i,:)= (rho* v_initial(i)* D_initial(i)/ mu);
        Ro(i,:)= v_initial / (2* v_t* sind(90)); % Rossby
            Number- li2001
        Fc_F= (((2*3.14*RPM (i))/60)^2* R * D_initial(i))/ (
            v_initial(i)^2);
end
%% Image Calibration-Slanted
%Reference Image Processing
figure
reference_length = 1; %mm
img = imread('Corrected_Calibration_Image.bmp');
bw = imadjust(rgb2gray(img),[0.2 0.5],[]);
bw_cropped=imcrop(bw);
imshow(bw_cropped)
Rmin=15;
Rmax=40;
[centersDark, radiiDark] = imfindcircles(bw_cropped,[Rmin
    Rmax],'ObjectPolarity','dark','EdgeThreshold', 0.2) ; %
    Finds first droplet    ----------------------
viscircles(centersDark, radiiDark,'LineStyle','--', '
    EdgeColor', 'b');
h = imdistline(gca, [centersDark(1)-radiiDark centersDark(1)+
    radiiDark] ,[centersDark(2) centersDark(2)]);
```

```
api = iptgetapi(h);
fcn = makeConstrainToRectFcn('imline',...
     get(gca,'XLim'),get(gca,'YLim'));
api.setDragConstraintFcn(fcn);
unit_length_pix_slanted = 2*radiiDark;
%%
Files=dir('Z:\TUBITAK 1001\Fluid Mechanics\Spreading
   Experiments\Smooth Glass\Article Data\Smooth\High Wen-Low
   Wet\26cm_500rpm_7_1_tilted\Spreading\Processed\New folder
   \*.jpg');
figure
[im crop_rect]=imcrop(imread(Files(1).name));
%%
Initial_frame= input('Enter the Frame Number which drop meets
    with surface: '); % Write the frame number manually(where
    drop meets with the surface)
Spreading_Frame=input('Enter the Frame Number which drop
   starts spread: ');
%%
for i=1:length(Files)
I= imread(Files(i).name);
I2=imcrop(I,crop_rect);
figure, imshow(I2)
stats_crop= regionprops(I2);
%% Contour Tracing
[B,L,N] = bwboundaries(I2,4);
stats= regionprops(L, 'all');
```

```
hold on
%% Define the second max area athe cropped area
for k=1:length(B)
  area(k)= stats(k).Area;
end
area= sort(area, 'descend');
%% Draw the boundary
for k =1: length(B)
    if stats(k).Area == area(1)
        boundary = B{k};
        AREA= (stats(k).Area * reference_length )/ unit_length_pix_slanted ; % mm2
        PERIMETER= (stats(k).Perimeter * reference_length) / unit_length_pix_slanted ; % mm
        EQV_DIAMETER=(stats(k).EquivDiameter * reference_length) / unit_length_pix_slanted; %mm
        Major_Axis=(( stats(k).MajorAxisLength * reference_length) / unit_length_pix_slanted); %%mm
        v_major= ((Major_Axis/2)/((Spreading_Frame-Initial_frame)*t_cam))/1000; %m/s
        Minor_Axis=((stats(k).MinorAxisLength * reference_length) / unit_length_pix_slanted);%mm
        v_minor=((Minor_Axis/2)/((Spreading_Frame-Initial_frame)*t_cam))/1000; %m/s
        Orientation=stats(k).Orientation;
        Eccentricity=stats(k).Eccentricity;
        Centroid=stats(k).Centroid;
```

```
            Spread_Factor_tan=Major_Axis/(D_initial*1000); % D was in m converted to mm
            Spread_Factor_rad=Minor_Axis/(D_initial*1000);
            %%
            % Parametric Ellipse Equation
            t = linspace(0,2*pi,100);
            a = (Major_Axis/2)*unit_length_pix_slanted;
            b = (Minor_Axis/2)*unit_length_pix_slanted;
            Xc = Centroid(1);
            Yc = Centroid(2);
            phi = deg2rad(-Orientation);
            x = Xc + a*cos(t)*cos(phi) - b*sin(t)*sin(phi);
            y = Yc + a*cos(t)*sin(phi) + b*sin(t)*cos(phi);
            plot(x,y,'c','Linewidth',1) % Plot the ellipse found from the major minor axis length
            plot(boundary(:,2), boundary(:,1), 'b', 'LineWidth', 2) % Plot the found boundary
        end
         end
Results(i,:)= [AREA PERIMETER EQV_DIAMETER Major_Axis Minor_Axis Spread_Factor_tan Spread_Factor_rad v_major v_minor];
Time (i,:)= ((Spreading_Frame-Initial_frame) * (1/f))*1000; % ms
nondim_Time(i,:)= ((Time(i)/1000)* v_initial)/ D_initial;  % Calculate with velocity of contact line Radial
Spreading_Frame=Spreading_Frame+1;
```

```
end
%% Plot Parameters
% Spreading Area
figure
plot(Time , Results(:,1), 'DisplayName', 'Spread Area')
set(gca,'FontSize',15, 'FontWeight','bold');
set(gcf,'PaperPosition', [0 0 1280/150 800/150])
title('Droplet Spreading Area vs. Time')
xlabel('Time(ms)','fontsize',15)
ylabel('Spreading Area (mm^2)','fontsize',15)
% legend(gca,'show', 'Location', 'NorthWest')
% legend('Location', 'NorthWest')
saveas(gcf, 'Droplet Spreading Area vs time', 'jpg')
%% Eq. Diameter
figure
plot(Time,Results(:,3), 'DisplayName', 'Equivalent Diameter')
set(gca,'FontSize',15, 'FontWeight','bold');
set(gcf,'PaperPosition', [0 0 1280/150 800/150]);
title('Droplet Spreading Equivalent Diameter vs. Time')
xlabel('Time(ms)','fontsize',15)
ylabel('Droplet Spreading Equivalent Diameter(mm)','fontsize'
    ,15)
% legend(gca,'show', 'Location', 'NorthWest')
% legend('Location', 'NorthWest')
saveas(gcf, 'Droplet Spreading Equivalent Diameter vs time',
    'jpg')
%% Major Axis Length
```

```
figure
plot(Time,Results(:,4), 'DisplayName', 'Major Axis Length')
set(gca,'FontSize',15, 'FontWeight','bold');
set(gcf,'PaperPosition', [0 0 1280/150 800/150]);
title('Major Axis Length vs. Time')
xlabel('Time(ms)','fontsize',15)
ylabel('Major Axis Length(mm)','fontsize',15)
% legend(gca,'show', 'Location', 'NorthWest')
% legend('Location', 'NorthWest')
saveas(gcf, 'Major Axis Length vs time', 'jpg')
%% Minor Axis Length
figure
plot(Time,Results(:,5), 'DisplayName', 'Minor Axis Length')
set(gca,'FontSize',15, 'FontWeight','bold');
set(gcf,'PaperPosition', [0 0 1280/150 800/150]);
title('Minor Axis Length vs. Time')
xlabel('Time(ms)','fontsize',15)
ylabel('Minor Axis Length(mm)','fontsize',15)
% legend(gca,'show', 'Location', 'NorthWest')
% legend('Location', 'NorthWest')
saveas(gcf, 'Minor Axis Length vs time', 'jpg')
%% Tangential Spread Factor vs nondimtim
figure
plot(nondim_Time,Results(:,6), '-c*','DisplayName', 'Spread
    Factor Tangential')
set(gca,'FontSize',15, 'FontWeight','bold');
set(gcf,'PaperPosition', [0 0 1280/150 800/150]);
```

```
title('Tangential Spread Factor vs. Non-dimensional Time')
xlabel('Non-dimensional Time','fontsize',15)
ylabel('Spread Factor Tangential','fontsize',15)
saveas(gcf, 'Tangential Spread Factor vs nondimtime', 'jpg')
%% Radial Spread Factor vs nondimtim
figure
plot(nondim_Time,Results(:,7),'-ro' ,'DisplayName', 'Spread Factor Radial')
set(gca,'FontSize',15, 'FontWeight','bold');
set(gcf,'PaperPosition', [0 0 1280/150 800/150]);
title('Radial Spread Factor vs. Non-dimensional Time')
xlabel('Non-dimensional Time','fontsize',15)
ylabel('Spread Factor Radial','fontsize',15)
saveas(gcf, 'Radial Spread Factor vs nondimtime', 'jpg')
```

# VITA

Gökhan Kayansalçik received the B.Sc. degree in Mechanical Engineering from Ozyegin University, Istanbul, Turkey in 2015 and he is currently pursuing the M.Sc. degree in Mechanical Engineering at Ozyegin University. His research interest includes multiphase flows and thermofluids.